Wide range speed sensorless vector control of synchronous reluctance motor with start up ability

Ahmad Ghaderi

Graduate School of Life Science and Systems Engineering Kyushu Institute of Technology

February, 2007

Acknowledgements

I wish to express my sincerest appreciation to Prof. Tsuyoshi Hanamoto who provided the chance to study in Japan, for his outstanding and endless support during the many years of research. Professor Hanamoto's invaluable comments, suggestion, and encouragement have been of the greatest help in this research.

I gratefully acknowledge the Japanese government and the Japanese ministry of education for providing the scholarship which enabled me to pursue this study at Kyushu Institute of Technology.

I am also indebted to Professor Teruo Tsuji for his deep insight and unfailing enthusiasm and constant support.

I wish to express my deepest sense of indebtedness to the members of the examination committee, Professors Hirokazu Yokoi, Professor Hideki Honda and Professor Ryuichi Oguro for their valuable comments.

I would also like to express my deepest gratitude to all my professors, Professor Yamakawa, Professor Ishi and professor Futami.

My thanks also go to Professor Hiroshi Tsukamoto dean of graduate school of life science and system engineering, Kyushu Institute of Technology, FAIS-Robotics Research Institute, Professor Godler from Kitakyushu University, Ms. Kaga and Ms. Watanabe and my friends.

Furthermore, I wish to thanks my colleagues in Hanamoto laboratory for their unlimited help during various stages of the research work.

Expression of graduate and apology are directed to the author's family whose encouragements have been the most influence support during the whole course of my education.

Contents

List of Figures

Dedicated to my parents and my wife.

Chapter 1

Introduction

Variable speed operation of ac machines are being incessantly innovated and have developed as a way to convert electric energy to mechanical work in a wide range of industrial application such as fans, pumps, elevators, paper and textile mills, electric vehicle and subway transportations, wind generation systems, servo and robotics, home applications, computer peripherals, steel and cement mills, ship propulsion, factory automation, etc [1]-[4]. This development is caused by progress made in various area including power and micro electronics, control systems, magnetic materials, microprocessors and modern communication technologies.

Inverter-fed synchronous motors are widely used in high-performance variable-speed drive systems. If the synchronous machine is supplied by a current-controlled voltage-source PWM inverter, then the stator currents are decided by the reference speed or reference electromagnetic torque. And the inverter drives the synchronous motor, so that the instantaneous stator currents follow their reference values. For high-performance drives it is possible to use various rotor configurations: rotor with permanent magnets, reluctance type, and electrically exited rotors [4]-[7].

There are basically three types of permanent-magnet synchronous machine. The permanent-magnet synchronous machine with surface-mounted magnet, inset magnets and buried magnet [6].

The synchronous reluctance motor (SYRM) is singly-salient synchronous motor where the symmetrical three-phase sinusoidally distributed stator winding are exited with balanced AC currents and there is a reluctance rotor. The three-phase stator winding are situated in the smooth but slotted stator bore. The reluctance rotor is made of steel laminations, it is salient-pole, but does not have any winding or magnet. The rugged simple structure, low cost manufacturing, possibility of high torque per unit volume, and the absence of rotor windings resulting in simple control

schemes and decreased losses make this motor an attractive candidate for numerous industrial and automotive applications [8-11].

1.1 Speed sensorless control of SYRM

In synchronous reluctance motor (SYRM), to synchronize the stator current vector with rotor position, determination of the rotor position is necessary. While speed sensors increase cost and size, the reliability of the system decreases because of noise effect. Hence recently much research has been done on the sensorless control of SYRM.

1.1.1 Previous researches

Several solutions proposed by researchers in literatures, in the following these solutions will be sketched.

The primary sensorless technique is based on the direct control of the motor load angle. Two solutions have been proposed, the former one [7] operates the inverter in the voltage-controlled mode by keeping V/f constant, torque angle is calculated from steady-state motor equation. The second one [13] calculate the torque angle by using dynamic equations on the basis of measured terminal quantities (voltages and currents) of the motor fed by a current-controlled voltage source inverter. In [14]-[16] closed-loop speed control has been implemented by estimating the rotor speed from the flux-linkage vectors angular velocity. These types of solutions are affected by motor parameters variation.

In [17] to estimate the magnitude, position, and speed of magnetizing-flux space vector, the spatial saturation third-harmonic voltage is utilized. It should be emphasized that this scheme requires the stator windings to be wye-connected and also there has to be access to the neutral point of stator windings. At low speeds problems arise due to the distorted third harmonic voltage [6]. On the other hand it requires motor operation in saturated condition and, as a consequence, it is not allowable for field weakening operation.

Due to rotor saliency, the inductances of the SYRM depend on the rotor position. Thus in some researches the rotor position is estimated by using inductance variations due to geometrical effects [18]-[23]. Some authors [18]-[21] proposed to detect rotor position at the zero crossing of the phase current by modifying the switching modulation. This method does not provide high performances, in particular at low speed, because of its low estimation update rate. In [22]-[23], the rotor position is estimated from the monitored rate of change of the stator currents. Although this method has good dynamic operation the estimation is depended on inductance. This estimation method can be used at low rotor speed, including zero speed, but the estimation accuracy decreases radically at higher speeds.

It is possible to estimate the rotor position together with other quantities (e.g. the load torque, speed) by using state observer like as extended Kaman filter or an extended lenbergure observer. Kalman-filter, state-observer and other sensorless control schemes based on application of

identification procedure allow low and zero speed operation, but they are strongly affected by motor parameter variations, or are too complex, and expensive to be used in low cost systems. Observer-based systems or Kalman filtering in real-time require a very fast signal processor specialized and optimized to perform complex mathematical calculations and manipulate large amount of data. And in some cases, wrong values for the noise covariance matrices (not correlated to the actual noise) as well as wrong initial value lead to instability [6], [24]-[26].

A recent solution makes use of artificial intelligence techniques (fuzzy logic, artificial neural network, fuzzy-neural network, etc.). However since it is possible to approximate any non-linear function with grate accuracy by using these techniques, a proper artificial intelligence system (in particular a neural network properly trained) is able to estimate motor position and speed [27], [28].

In [5] the sensorless speed control methods are categorized in two major types. At first category, AC machine is modeled by its state equations. A sinusoidal flux density distribution in the air gap is then assumed, neglecting space harmonics and other secondary effects. The approach defines the class of fundamental models. They are either implemented as open loop structures, like the stator model, or as closed loop observers.

In the second method to exploit machine anisotropy, other frequencies than the fundamental frequency is injected to motor and the field angle or the rotor position angle is identified using the response of the motor [29]-[31].

Algorithms that rely on the fundamental machine model excel through their simplicity, even if more sophisticated and detailed models are implemented for the components of the drive system. Additional hardware for the acquisition of the machine terminal voltage can be spared when modeling the inverter as a nonlinear component.

1.1.2 Effects of DC-offset, parameter variations and inverter nonlinearity

In some methods, SYRM is modeled by its state equations. A sinusoidal flux density distribution in the airgap is then assumed, neglecting space harmonics and other secondary effects. This approach defines the class of fundamental models.

Although using fundamental models [13] to estimate angles is the most straightforward approach and has several advantages, immunity to noise, offset and drift should be achieved using appropriate techniques otherwise measurement noise and DC offset causes an increasing error in this estimator. Therefore, the estimation of rotor angle and speed will be not correct. These incorrect quantities will be compared with references variables and cause an unwanted increasing oscillation in flux and torque.

Although using a LPF with a large time constant instead of the pure integrator prevents the output from increasing without bounds, this integrator model becomes inaccurate at low speeds, because the gain and angle of a LPF and a pure integrator will be different, when the frequency reduces to around LPF corner frequency. Thus this method can not solve the above mentioned problem at a low speed region [5]-[6] .

Use of programmable cascaded low pass filters (PCLPF) instead of pure integrators is another alternative method to reduce drift-error and it has previously been applied to the sensorless control of induction motors [32]. PCLPF consists of some low pass filter blocks and an amplifier block in cascade form. But PCLPF may cause other drawbacks at low speeds. These problems are explained by authors in their previous research [33]. However, in this research, an adapted PCLPF was used in the SYRM by using a novel method to avoid of its drawbacks at low speeds.

On the other hand in this method to estimate stator flux linkages, stator resistance must be defined precisely otherwise the rotor angle estimation is not valid. The estimation of the load angle also requires the motor inductances. Thus a proper method for identifying motor parameter is essential [6], [34]-[37]. On the other hand this identified parameter is used in calculation of decoupling signals [6], [38]. In a VSI-fed SYRM, the stator voltages can be reconstructed by utilizing the switching signals of the inverter and the monitored DC link voltage. But the power transistors used in three-phase PWM VSI as switching devices, have finite turn-off times and there is a need to insert a time delay after switching device off and the other device on in one inverter leg. Due to present of the dead time, the output-voltage space vector of the inverter is not equal to the desired voltage space vector. Thus this error voltage should be considered in reference voltage calculation [6], [39].

1.2 Objective of the dissertation

1.2.1 Rotor angle estimation for SYRM at low speed and near zero speed

As mentioned in 1.1.2, although open loop fundamental models have several advantages their limits is at near zero frequency. The rotor induced voltage is then low , thus the dc offset and drifts effects that arise from analogue signal measurement, can cause an increasing error in the pure integrator used this type of estimator and should be avoided [5]-[7].

Although the use of three stages programmable cascaded low pass filter (PCLPF) has previously been applied to sensorless control of induction motors [32],[40], in this paper, this filter is adapted to estimate phase angle at low speed and near zero speed area in SYRM.

To estimate rotor angle at low speed, modified programmable cascaded low pass filter (MPCLF) is presented by authors [41]-[43]. The problems of PCLPF are reduced because the PCLPF gain is eliminated in phase angle calculation.

In the next stage, the range of rotor angle calculation is expanded from near zero speed to high speed by proposing extended programmable cascaded low pass filters (EPCPLF) [44]. The performance of these filters is improved considerably by extending their stages and reduces its gain. Because the proposed method reduces the PCLPF drawbacks at low speed, effectively, the rotor angle estimation at very low speed is valid and thus, sensorless control at near zero speed is possible.

Although the rotor angle estimation using EPCPLF is possible at near zero speed, but its necessary calculation is more MPCLPF. Thus we suggest using EPCLPF in very low speed precise

application while MPCPLF can be used in low speed application when we have limitation in hardware capacity (memory and pressures).

1.2.2 Parameter identification using block pulse functions

In open loop fundamental models, as the stator frequency reduces at lower speed, the stator voltage reduces almost in direct quantity, while the resistive voltage is maintains its order of magnitude. It becomes the significant term at low speed. Thus, any variation in motor parameters will disorder position estimation. The effect of stator resistance variation is more important in low speed regions, because the inverter voltage decreases in relation to stator resistance voltage and the resistance voltage dominates the integrator input in low speed [5]-[6]. Therefore these need to be tracked to maintain the system stable at low speed.

To avoid mentioned drawbacks an online parameter identification method which does not depend on estimation accuracy is suggested [42], [45].

In the proposed method, motor parameter identification is done using a block pulse function (BPF) instead of the Euler method which is used in [35]-[37]. The Block Pulse Functions (BPF) is a set of orthogonal functions with piecewise constant values and to use the BPF approximation, differential equations are transformed approximately into their corresponding algebraic forms based on the operation rules of BPF, so that the numerical solutions obtained more directly[46]. And it saves calculation time compared with the other numerical analysis method, such as a Runge-Kutta algorithm [47].

It is shown although the identified parameter is not dependent on angle difference of actual *d-q* axes and the estimated $\delta - \gamma$ axes [35]-[37]. Hence, in this method, parameter identification is not affected by position estimation accuracy.

1.2.3 Motor startup from zero speed

At the standstill condition, the rotor angle is assumed rotating at reference speed, and because the proposed method can estimate rotor angle at very low speed area, the estimated and actual rotor angle converge rapidly and the motor startup is done without the torque jerk caused by transition from the standstill mode to the vector control mode which usually is used in sensorless control of SYRM.

1.2.4 Wide range of speed sensorless vector control of SYRM

A wide range speed sensorless vector control will be achieved, using a combination of MPCLPF or EPCLPF and BPF-based parameter identification. Since the motor control strategy can be determined by regulating stator current in the d axis, several close loop self control methods, like as constant d-axis current control, maximum torque/ampere control and maximum power factor control are achieved using the identified parameters [45]. Also the startup is possible without the torque jerk.

To achieve the proposed method, the experimental setup employs a PC-based system with real time Linux (RTLinux) [48] as an operating system. RTLinux can satisfy the system hardware and software constraints and also real time control can be achieved using this operating system. To acquire the data from the sensors and to send the gate signals to the system, an interface was designed by the Complex Programmable Logic Device (CPLD). The experimental results show the proposed method performs well and speed and angle estimation is correct in a wide range of speeds.

1.3 Organization of the dissertation

Chapter 2

In this chapter at fist, the synchronous reluctance motor is introduced. A brief history of this motor is presented. Various type of SYRM includes flux barriers, axially laminate and segmental rotor is explained. The effect of motor saliency on the power factor, torque density and efficiency and its limitation is explained. The recent developed in SYRM is illustrated. Equations of SYRM in stationary reference frame are presented and this equations and transformation equation are used to extract machine equations in rotating reference frame. Then the equations of torque are extracted. Movement mechanism in SYRM is explained and rotor-oriented vector control for SYRM includes Current-type control and combined current-voltage controls are introduced. Finally various types of Vector control strategies are expressed.

Chapter 3

In this chapter the phase angle calculation using armature voltages and currents is presented and its block diagram is explained, then the effect of DC-offset on the accuracy of this estimation is surveyed. PCLPF is introduced and its drawbacks are explained. Modified PCLPF and its block diagram are presented and its benefits in low speed area are explained. To estimate phase angle at very low speed and near zero speed extended PCLPF (EPCLPF) is suggested. The effect of EPCLPF stages in DC-offset calculation is shown. Then the equations of rotor angle calculation are presented. And finally the conclusion of chapter is explained.

Chapter 4

The effect of the parameter variation on sensorless vector control and its compensation method are considered. At first the effect of stator resistance variations in phase angle calculation is explained and its effect in low speed is surveyed. The inductance importance in load angle estimation and decoupling signals is shown. Our proposed identification is presented. And block pulse function is introduced. Then the equations of proposed parameter identification method are discussed and it is shown that this method is not affected by position estimation accuracy. Finally the chapter conclusion is explained.

Chapter 5

In chapter 5 the proposed sensorless vector control is presented and its block diagram is explained. And it is shown that MPCLPF and EPCLPF and online parameter identification ,that are explained in previous chapters, are employed in this block diagram. To startup motor in stand still condition a novel method which uses EPCLPF is suggested. The block diagram of proposed method is presented and its operation is explained.

The block diagram of practical system configuration is presented and the proposed experimental setup is presented and its hardware and software is discussed. Then the practical result of sensorless control and proposed parameter identification is presented.

The result of MPCLPF estimator, which was explained in chapter 3, in a wide range of speed is experienced and its stability is tested by adding an artificial DC-offset to measured currents. The transient response of sensorless MPCLPF is presented and the result of two close loop control strategy is shown. Finally the effect of EPCLPF which includes 6 stages LPF filter is presented in low speed and very low speed area. And it is shown that estimation is achieved even near zero speed.

The step responses of reference speed and torque load are evaluated, and the result of direction changed is investigated.

The result of motor start up ability is presented and the effect of low pass filter stages in estimation accuracy is studied.

Chapter 6

Major conclusions that can be drawn from this dissertation are given in this chapter.

Chapter 2

Principle of vector control of synchronous reluctance motors

2.1 Summary

In this chapter at first, the synchronous reluctance motor is introduced. A brief history of this motor is presented. Various type of SYRM includes flux barriers, axially laminate and segmental rotor is explained. The effect of motor saliency on the power factor, torque density and efficiency and its limitation is explained. The recent developed in SYRM is illustrated. Equations of SYRM in stationary reference frame are presented and this equations and transformation equation are used to extract machine equations in rotating reference frame. Then the equations of torque are extracted. Movement mechanism in SYRM is explained and rotor-oriented vector control for SYRM includes Current-type control and combined current-voltage controls are introduced. Finally various types of Vector control strategies are expressed.

2.2 Synchronous reluctance motor

Synchronous reluctance motors (SYRM) are a type of synchronous machines that have salient poles without any filed winding or permanent magnet on the rotor. These motors are low cost, rugged, and capable of operating at very high speeds. The structure of SYRM is shown in Fig. 2.1.

SYRM were discussed as early as 1932 (the early versions with conventional reluctance rotor are characterized by high torque pulsation, low torque density, very low power factor and efficiency. This type of motors was developed in the UK by professor Lawrenson in the 1960s and by Honsinger in the USA.

A synchronous reluctance motors (SYRM) can have various rotor configuration. In earlier constructions, rotor saliency was achieved by removing certain teeth from the rotor of a

conventional squirrel cage. Such synchronous reluctance machines with low output power have been used for a long time and their inferior performance combined with their relatively high price have result in a limit use. However, as a result of recent developments, more reliable and robust new construction exist, these have basically three types of the rotors; segmental, flux barrier, and axially laminated rotors. In the SYRM with segmental rotor, saliency ratios of 6-7 have been obtained. By using multiple segmental structures, the saliency ratio can be increased. In the SYRM with axially laminated rotor, the rotor is made of conventional axial laminations bent into U or V shapes and stacked in the radial direction. With this structure it is possible to produce very high saliency ratios of 9-12 have been obtained [6]. This also leads to fast torque response. A flux barrier type synchronous reluctance motor has a stator with a plurality of spaced slots and teeth and a rotor with a plurality of flux barriers [12]. The rotor shape of a flux barriers SYRM is shown in Fig.2.2.

Although, the power factor, torque density and efficiency of SYRM increase when the saliency ratio is high, it should be that there is a physical limit to the maximum of saliency ratio which is curtained by ratio of synchronous inductance and leakage inductance. In general, a SYRM is characterized by torque pulsations, vibration and acoustic problems. However there are several attentions to solve these problems and improve the motor behavior in recent researches [49]-[55].

The resent developed SYRM have high saliency in compared to traditional models, which has significantly improved torque density, power factor, and efficiently to the point where they are almost comparable to those of an induction motor. However, it is distinct advantage over induction machines that reluctance machines at exactly the synchronous speed (which is solely, determined by stator the stator excitation frequency and the number of poles) and there are no rotor currents. These are important aspects in many industrial applications [6]-[7].

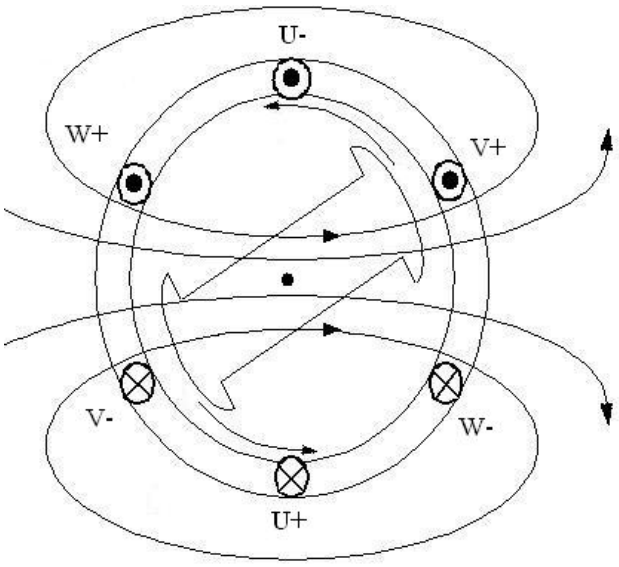

Fig 2.1 Structure of SYRM

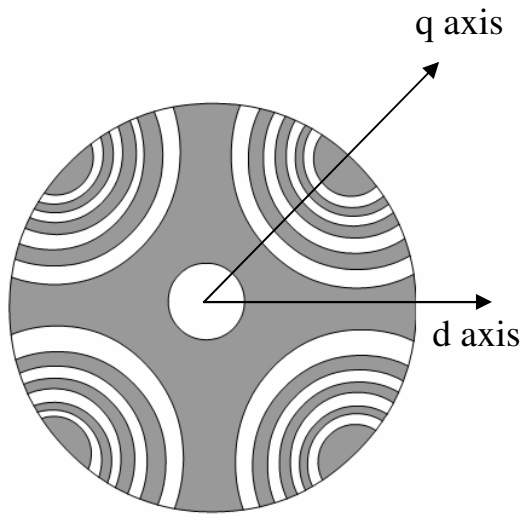

Fig 2.2 flux barriers SYRM

2.2.1 Synchronous reluctance motor equations in stationary reference frame

The three-phase voltage equations of the synchronous reluctance motor can be described by equations given below in stationary reference frame [56]-[57].

$$\begin{bmatrix} v_{as} \\ v_{bs} \\ v_{cs} \end{bmatrix} = \begin{bmatrix} R_a & 0 & 0 \\ 0 & R_a & 0 \\ 0 & 0 & R_a \end{bmatrix} \begin{bmatrix} i_{as} \\ i_{bs} \\ i_{cs} \end{bmatrix} + \frac{d}{dt} \begin{bmatrix} \psi_{as} \\ \psi_{bs} \\ \psi_{cs} \end{bmatrix} \tag{2-1}$$

Where v_{as}, v_{bs} and v_{cs} are the motor phase voltages, R_a is the stator winding resistance ψ_{as}, ψ_{bs} and ψ_{cs} are the flux linkages of three phases. The flux linkages can be expresses as:

$$\begin{bmatrix} \psi_{as} \\ \psi_{bs} \\ \psi_{cs} \end{bmatrix} = \begin{bmatrix} L_{asas} & L_{asbs} & L_{ascs} \\ L_{bsas} & L_{bsbs} & L_{bscs} \\ L_{csas} & L_{csbs} & L_{csc\,s} \end{bmatrix} \begin{bmatrix} i_{as} \\ i_{bs} \\ i_{cs} \end{bmatrix} \tag{2-2}$$

Where L_{asas}, L_{bsbs} and L_{cscs} are machine self inductance and L_{asbs}, L_{ascs}, L_{bsas}, L_{csas}, L_{bscs} and L_{csbs} are defined as mutual inductances between motor phases and is calculated as follow :

$$L_{asas} = L_{ls} + L_A - L_B \cos 2\theta_r \tag{2-3}$$

$$L_{bsbs} = L_{ls} + L_A - L_B \cos 2(\theta_r - \frac{2\pi}{3}) \tag{2-4}$$

$$L_{asbs} = -\frac{1}{2} L_A - L_B \cos 2(\theta_r - \frac{\pi}{3}) \tag{2-5}$$

$$L_{ascs} = -\frac{1}{2} L_A - L_B \cos 2(\theta_r + \frac{\pi}{3}) \tag{2-6}$$

$$L_{ascs} = -\frac{1}{2} L_A - L_B \cos 2(\theta_r + \frac{\pi}{3}) \tag{2-7}$$

$$L_{bscs} = -\frac{1}{2} L_A - L_B \cos 2(\theta_r + \pi) \tag{2-8}$$

Where L_{ls} and θ_r represents the leakage inductance of the phase and rotor angle respectively and L_A and L_B are calculated as follow.

$$L_A = \mu_0 r l N_s^{\,2} (\frac{\pi}{8})(\frac{1}{g_{min}} + \frac{1}{g_{max}}) \tag{2-9}$$

$$L_B = \mu_0 r l N_s^{\,2} (\frac{\pi}{8})(\frac{1}{g_{min}} - \frac{1}{g_{max}}) \tag{2-10}$$

Where g_{min} represents the d-axis equivalent air gap and g_{max} represents the q-axis equivalent air gap and r, l, and N_s denote the rotor radius, the core length and the number of turns in series per phase.

With assumption of symmetrically for machine and using the three phase to two phase transformation (2-1) lead to (2-11).

$$\begin{bmatrix} v_\alpha \\ v_\beta \end{bmatrix} = R_a \begin{bmatrix} 1 & 0 \\ 0 & 1 \end{bmatrix} \begin{bmatrix} i_\alpha \\ i_\beta \end{bmatrix} + \frac{d}{dt} \begin{bmatrix} \psi_\alpha \\ \psi_\beta \end{bmatrix} \tag{2-11}$$

Where v_α, v_β, i_α, i_β, ψ_α and ψ_β are the two phases voltages, currents and flux in stationary reference frame.

From the (2-11) the fluxes in stationary reference frame can be calculated as follow:

$$\psi_\alpha = \int (v_\alpha - R_a i_\alpha) dt \tag{2-12}$$

$$\psi_\beta = \int (v_\beta - R_a i_\beta) dt \tag{2-13}$$

$$\psi_s = \sqrt{\psi_\alpha^2 + \psi_\beta^2} \tag{2-14}$$

Where ψ_s is the motor flux.

The motor torque (T_e) is produced by effect of rotor reluctance.

$$T_e = \frac{3}{2} P(\psi_\alpha i_\beta - \psi_\beta i_\alpha) \tag{2-15}$$

Where P is the number of motor poles.

2.2.2 Synchronous reluctance motor equations in rotating reference frame

It is seen in equations (2-3)-(2-8) show the machine inductances are functions of speed, whereupon the voltage equations that describe the performance of asynchronous reluctance machine are time varying except when the rotor is in standstill.

To eliminate time-varying inductance in the analysis of ac machines, the stator variables are transformed to a frame or reference fixed in the rotor using park equations. Although changing of variables are used to make inductances time invariant, the all ac variables (for example 60Hz) are transformed to dc variable and thus the sampling frequency could be decreased, whereupon the necessary calculation decreases effectively. As another advantage the fluxes in rotating reference frame there is no couple between its axes (d-q).

The axes of a SYRM are shown in Fig.2.3, and Fig 2.4 shows the relation between variables in, stationary and rotating reference frames.

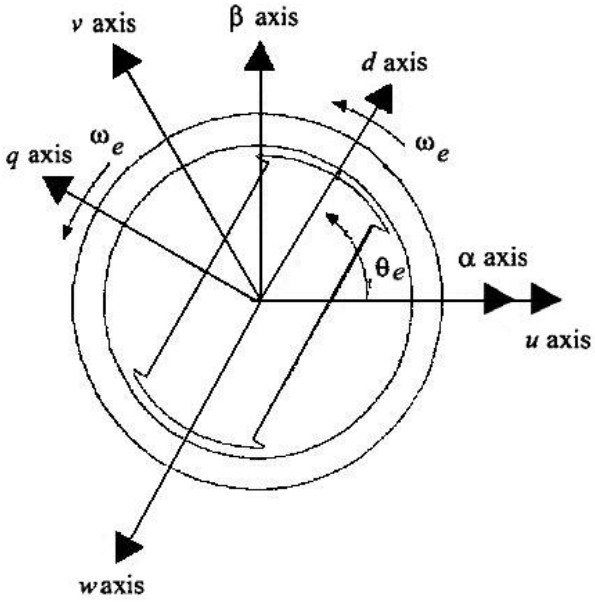

Fig 2.3 Axes of a SYRM

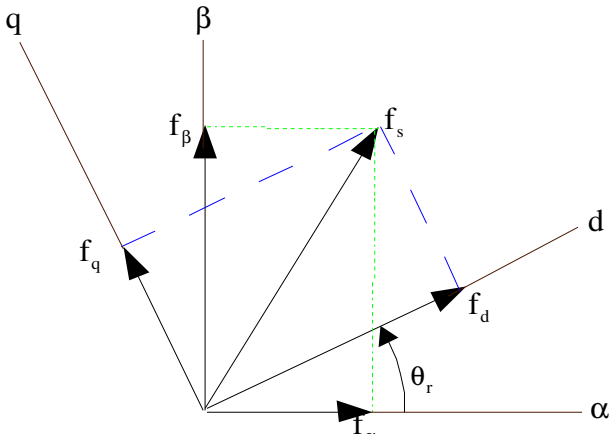

Fig 2.4 Transformation between reference frames

These figures are used to extract transformation equations which is shown in (2-16) and (2-17).

$$\begin{bmatrix} f_\alpha \\ f_\beta \end{bmatrix} = \begin{bmatrix} \cos\theta_r & -\sin\theta_r \\ \sin\theta_r & \cos\theta_r \end{bmatrix} \begin{bmatrix} f_d \\ f_q \end{bmatrix} \tag{2-16}$$

$$\begin{bmatrix} f_d \\ f_q \end{bmatrix} = \begin{bmatrix} \cos\theta_r & \sin\theta_r \\ -\sin\theta_r & \cos\theta_r \end{bmatrix} \begin{bmatrix} f_\alpha \\ f_\beta \end{bmatrix} \tag{2-17}$$

Where θ_r, f_α, f_β and f_α, f_β are rotor angle, variables in stationary reference frame and variables in rotating reference frame respectively.

The voltage equations of motor in rotatinng refrence frame is achived in (2-18) using (2-11) and (2-16).

$$\begin{bmatrix} v_d \\ v_q \end{bmatrix} = \begin{bmatrix} R_a + pL_d & -\omega_{re}L_q \\ \omega_{re}L_d & R_a + pL_d \end{bmatrix} \begin{bmatrix} i_d \\ i_q \end{bmatrix} \tag{2-18}$$

where p, ω_{re} are differential operator and stator frequency respectivly. And L_d and L_q are defined as motor inductances, and calculated as follw :

$$L_{mq} = \frac{3}{2}(L_A - L_B) \tag{2-19}$$

$$L_{md} = \frac{3}{2}(L_A + L_B) \tag{2-20}$$

$$L_q = L_{ls} + L_{mq} \tag{2-21}$$

$$L_d = L_{ls} + L_{md} \tag{2-22}$$

Where L_{mq} and L_{md} are magnetizing inductances. The torque in rotating reference frame can be calculated as (2-23) and (2-24).

$$T_e = \frac{3}{2}(\frac{P}{2})(\frac{L_d - L_q}{L_d L_q})\psi_q \psi_d \tag{2-23}$$

$$T_e = \frac{3}{2}(\frac{P}{2})(L_d - L_q) i_q i_d \tag{2-24}$$

Where $\psi_d = L_d i_d$ and $\psi_q = L_q i_q$.

This equation indicates that torque can be controlled by i_q, i_d or both components. Equation (2-24) can also be written in the form [7].

$$T_e = \frac{3}{2}(\frac{P}{2})(\psi_d i_q - \psi_q i_d) \tag{2-25}$$

2.3 Vector control of synchronous reluctance motor

Since the machine does not have a starting torque when exited from a constant frequency conventionally, it is necessary to have a cage winding in a reluctance machine. Although the modern reluctance motor drives operate without a rotor cage.

By using the cage winding, the machine runs up to synchronous speed by induction motor action where the rotor locks into synchronism with the field product by the motor. For sinusoidal stator excitation, at synchronous speed the only role of the cage winding is to damp the oscillations in the rotor speed. However, in modern SYRM drives, the variable stator excitation is used. Thus it is not necessary to have a rotor cage for starting purpose, since the excitation can be controlled in such a way that the motor is always kept in synchronism. Reluctance machines with cageless rotors lead to a reduction of rotor losses, improved efficiency, higher power factor, and higher torque/weight ratio [7]-[8].

The SYRM utilizes the principle that electromagnetic torque is produced to minimize the reluctance of magnetic paths. The three-phase stator currents produce a rotating air-gap flux. When the rotor rotates in synchronism with the air-gap flux, torque is produced which tries to align the minimum reluctance path of the rotor with the rotating air-gap flux. When a load torque is present, the rotor begins to lag the rotating air-gap flux producing a misalignment of the minimum reluctance path and the rotating air-gap flux. Thus electromagnetic torque is produced to minimize the reluctance which tries to maintain alignment. When this torque is equal and opposite to the load torque on the rotor, the rotor will again rotate with synchronous speed.

The SYRM drive requires the information on the rotor position for closed-loop control, but this information is in addition requires for starting purpose as well. However as mentioned in 1.1.2 speed and position information can be obtained without using speed and position sensor for several methods. Both vector control and direct torque control techniques can be applied to SYRM. For rotor-oriented vector control, (2-24) or (2-25) can be used. Two control strategies will be discussed bellow: current control and combined current-voltage control.

2.3.1 Current-type control

In a vector-controlled SYRM drive, where the motor is supplied by a current-controlled PWM inverter, and where rotor-oriented control is performed, independent control of the torque and flux (torque producing stator current and flux producing stator current) can be achieved by the current-type control scheme.

2.3.2 Combined current-voltage control

In this thesis the rotor oriented control of the SYRM is achieved, by using combined current and voltage control method. When such method is used, delays in AC current and saturation at high speeds can be avoided. The machine is supplied by a PWM voltage source inverter and is current controlled along the direct (d) and quadrature (q) axes of the rotating reference frame fixed to the rotor.

2.4 Vector control strategies

Several close loop self-control methods for vector control of SYRM can be achieved. Although these methods are defined as vector control because of the independent control of i_d and i_q components of stator current and vector transformation, they are not truly vector control because there is mo orientation with machine flux.

2.4.1 Constant d-axis current (i_d) control

In this simple control method, the d axis current is kept constant and the q-axis current is controlled to torque equation can be written in this form

$$T_e = \frac{3}{2}\left(\frac{p}{2}\right)\left(1 - \frac{L_q}{L_d}\right)\psi_d i_q \qquad (2\text{-}26)$$

This equation indicates that the torque is proportional to the product of ψ_d and i_q, and its polarity can be reversed by i_q polarity. The magnetizing current reference is constant in the constant torque region but it is reduced beyond the base speed for extended speed control operation.

2.4.2 Fast torque response control

In this control strategy, it is desired to have the fast response of the drive. The fast torque response will be achieved when the equations (2-27) is valid.

$$\frac{i_q}{i_d} = \frac{L_d}{L_q} \qquad (2\text{-}27)$$

In this situation, the maximum torque expression can be derived as (2-28)

$$T_e = \frac{3}{2}(\frac{p}{2})(\frac{L_d L_q (L_d - L_q)}{L_d^2 + L_q^2})(i_d^2 + i_q^2) \quad (2\text{-}28)$$

The saturation effects of L_q can be compensated in the torque computation, if desired.

2.4.3 Maximum torque/ampere response control

Maximum torque/ ampere response control strategy, which tends to give maximum drive efficiency, is achieved when $i_d = i_q$.

2.4.4 Maximum power factor control

To maintain the maximum power factor, ratio of d-axis and q-axis currents should always be equal to (2-29) [7].

$$\frac{i_q}{i_d} = \sqrt{\frac{L_d}{L_q}} \quad (2\text{-}29)$$

Chapter 3

Rotor angle estimations for synchronous reluctance Motor

3.1 Summary

In this chapter the phase angle calculation using armature voltages and currents is presented and its block diagram is explained, then the effect of DC-offset on the accuracy of this estimation is surveyed. Programmable cascaded low pass filter is introduced and its drawbacks are explained. Modified PCLPF and its block diagram are presented and its benefits in low speed area are explained. To estimate phase angle at very low speed and near zero speed extended PCLPF is suggested. The effect of EPCLPF stages in DC-offset calculation is shown. Then the equations of rotor angle calculation are presented. And finally the conclusion of chapter is explained.

3.2 Introduction

In Synchronous reluctance motors because the stator current vector and rotor position should be synchronized, the determination of the rotor position is essential. But because the speed sensors need the extra hardware and increase the cost and the size, and the reliability of the system decreases because of noise effect, sensorless control of SYRM has been mentioned in recent researches.

In a SYRM, because the rotor follows the flux, the position of rotor and fluxes are changed together and it is possible to extract the rotor position by detecting of flux position. Therefore in this method the rotor position is estimated using flux linkage.

As mentioned in chapter 1, flux calculation using fundamental models to estimate angles is the most straightforward approach and has several advantages.

In this approach, torque (T_e), speed (ω_r) and flux linkage phase angle (ρ_s), in both transient and steady states, is calculated by using the estimated stator flux linkage (ψ_s), and its components (ψ_α, ψ_β) in stationary reference frame. The equations of these calculations are shown in (3-1)-(3-5) [5]-[7].

$$\psi_\alpha = \int (v_\alpha - R_a i_\alpha) dt \tag{3-1}$$

$$\psi_\beta = \int (v_\beta - R_a i_\beta) dt \tag{3-2}$$

$$\rho_s = \tan^{-1}\left(\frac{\psi_\beta}{\psi_\alpha}\right) \tag{3-3}$$

$$\psi_s = \sqrt{\psi_\alpha^2 + \psi_\beta^2} \tag{3-4}$$

$$T_e = \frac{3}{2} p(\psi_\alpha i_\beta - \psi_\beta i_\alpha) \tag{3-5}$$

Where p is number of poles. And v_α, v_β and i_α, i_β are defined as motor voltages and currents in stationary reference frame.

The block diagram of phase angle estimator base on above equations is shown in Fig. 3.1.

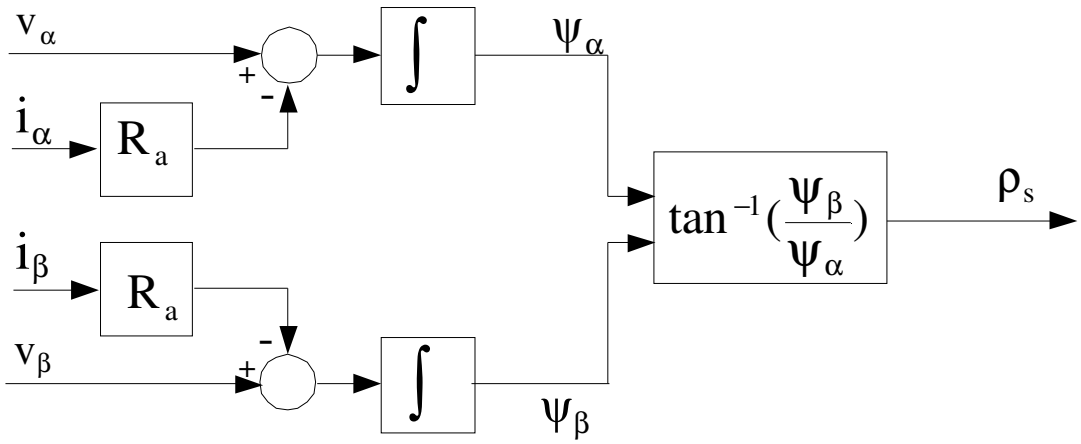

Fig 3.1 Phase angle estimation

3.3 DC offset problem in estimator

As seen in Fig.3.1 there is not any feedback in estimator and any noise and DC offset in measured stator currents and voltages make an increasing error in output of pure integrators used in this estimator. Thus a runaway drift will appear at estimated fluxes in (3-1) and (3-2), and consequently estimated flux linkage phase angle and torque, calculated at (3-3) and (3-5), are not valid. These invalid quantities are compared with references variables and cause an unwanted increasing oscillation in flux and torque.

DC offset may be produced in every part of the system like as voltage or current sensors, filters, or signal amplifiers. However there are various methods to reduce DC offset in measured voltages and currents [6], [58]-[59] but complete elimination is impossible.

Although using a LPF with a large time constant instead of the pure integrator prevents the output from increasing without bounds, this integrator model becomes inaccurate at low speeds, because the gain and angle of a LPF and a pure integrator will be different, when the frequency reduces to around LPF corner frequency. This causes an increasing error of the estimated field angle as the stator frequency reduces, which finally cause instability in motor control.

3.4 Programmable cascaded low pass filter

Programmable cascaded low pass filter (PCLPF) is an approach for solve DC offset problem in sensorless vector control of induction motors that proposed in 1997 [32]. This filter consists of some blocks of low pass filter and an amplifier block in cascade form instead of pure integrator to make a gain and angle like a pure integrator. Because LPF blocks and each LPF decrease the effect of the DC-offset, the DC-offset effect in the PCLPF output decreases effectively.

On the other hand the cutoff frequencies of low pass filters and amplifier gain are changed by the stator frequency thus PCLPF acts as a pure integrator which can solve the drift due to DC offset in measured values.

3.4.1 Equations of PCLPF

The transfer function of a three stage low pass filer which defined by H(s) is represented in (3-6)-(3-8).

$$\tau = \frac{1}{\omega_e}\tan(\frac{\pi}{6}) \tag{3-6}$$

$$G = \frac{1}{\omega_e}\sqrt{\left[1+(\omega_e\tau)^2\right]^3} \tag{3-7}$$

$$H(s) = G\left(\frac{1}{\tau s+1}\right)^3 \tag{3-8}$$

Where, ω_e,G and τ are the supplied voltage frequency, the PCLPF gain and the time constant of cascaded filters respectively.

As a result, the estimated fluxes of both axes ($\hat{\psi}_\beta$, $\hat{\psi}_\alpha$) and phase angle ($\hat{\rho}_s$) are calculated as follows using (3-8) instead of (3-1)-(3-3).

$$\hat{\psi}_\alpha = \left(v_\alpha - R_a i_\alpha\right)H(s) \tag{3-9}$$

$$\hat{\psi}_\beta = \left(v_\beta - R_a i_\beta\right)H(s) \tag{3-10}$$

$$\hat{\rho}_s = \tan^{-1}\left(\frac{\hat{\psi}_\beta}{\hat{\psi}_\alpha}\right) \tag{3-11}$$

3.4.2 Evaluation of PCLPF function

By recalculate of PCLPF equations, (3-12) and (3-13) can be written instead of (3-6) and (3-7) as the follow.

$$\tau = \frac{\sqrt{3}}{3\omega_e} \tag{3-12}$$

$$G = \frac{8}{3\sqrt{3}}\frac{1}{\omega_e} \tag{3-13}$$

And the phase lag and gain of the PCLPF at each frequency is calculated shown in the following equation.

$$H(j\omega) = \left(\frac{1}{1+\frac{\sqrt{3}}{3\omega_e}j\omega_e}\right)^3 \times \frac{8}{3\sqrt{3}} \times \frac{1}{\omega_e} = \frac{1}{j\omega_e} \tag{3-14}$$

$$H(j\omega) = \frac{1}{\omega_e}\angle\left(-\frac{\pi}{2}\right) \tag{3-15}$$

As seen in equation (3-15) the gain and phase angle of this system is equal with pure integrator but also there are some problems in this method.

a) In the equation (3-15) ω_e is appeared at denominator and the system output increase infinitely when motor is at standstill. Therefore this method needs extra system for starting up.

b) As shown in (3-13) the amplitude of gain increases when the motor speed decrease. And in near zero speed this value is vast. On the other hand, because of inverter nonlinearity in low speeds the ratio of voltage and gain and consequently $H(s)$ is not same, thus the calculated flux using (3-9) and (3-10) is not exact in low speed area and it leads to a calculation error in rotor angle estimation.

c) Filter output to a DC signal V_{dc} equals GV_{dc}. Then DC offset in the output depends on frequency and increase when frequency decreases. Therefore there are large amounts of DC offset at the estimated flux in d and q axes when the motor speed is low.

As a result, the estimated value will be invalid and sensorless control will not be achieved at low speeds [33], [42].

3.5 Rotor angle estimation using modified and extended programmable cascaded low pass filter

In this thesis, to avoid the PCPLF disadvantages two method is proposed. In first method which is called modified programmable low pass filter (MPCLPF), the estimation accuracy is improve by eliminating of gain in phase angle calculation. While in the further method which can be applied for

very low speed area the estimator behavior is modified by gain eliminating and extending of LPF stages. Thus this method is called extended PCLPF (EPCLPF).

3.5.1 Modified PCLPF

As mention in 3.3.1 the gain of the PCLPF increases vastly, when speed decreases. And it leads to an invalid estimation for phase angle in low speed region.

To solve this problem the output is extracted just after three stages of the LPF, in calculation of stator flux linkage phase angle (ρ_s). Because gain (G) is a common factor in ψ_α and ψ_β, it can be eliminated in phase angle calculation. Hence $H'(s)$, which is defined as MPCLPF transfer function and shown in (3-16) is used instead of (3-8).

$$H'(s) = \left(\frac{1}{\tau s+1}\right)^3 \tag{3-16}$$

And in equation (3-19), in order to calculate the output of the MPCLPF, Which is shown in (3-17) and (3-18), is used instead of (3-9) and (3-10).

$$F_\alpha = (v_\alpha - R_a i_\alpha) H'(s) \tag{3-17}$$

$$F_\beta = (v_\beta - R_a i_\beta) H'(s) \tag{3-18}$$

$$\hat{\rho}_s' = \tan^{-1}\left(\frac{F_\beta}{F_\alpha}\right) \tag{3-19}$$

Where F_α and F_β are defined as the output of the third LPF in the α and β axes, respectively.

The block diagram of rotor angle calculation using modified programmable cascaded low pass filters is shown in Fig.3.2.

Where $\delta, \rho_s, \omega_e, F_\alpha$ and F_β are load angle , phase angle , supplied voltage frequency , and the output of the sixth programmable LPF respectively .

3.5.2 Extended PCLPF

As mentioned previously, reduce the DC offset is effective way for the sensorless control in the low speed region [44] and because DC offset in the output depends on gain of the PCLPF, to reduce it, gain should be reduced. Here the relationship between the amplitude of the gain and the number of the PCLPF is considered. For a n stages LPF, the time constant of the filters, gain and transfer function are calculated in (3-20)-(3-22).

$$\tau = \frac{1}{\omega_e}\tan\left(\frac{\pi}{2n}\right) \tag{3-20}$$

$$G = \frac{1}{\omega_e}\sqrt{\left[1+(\omega_e\tau)^2\right]^n} \tag{3-21}$$

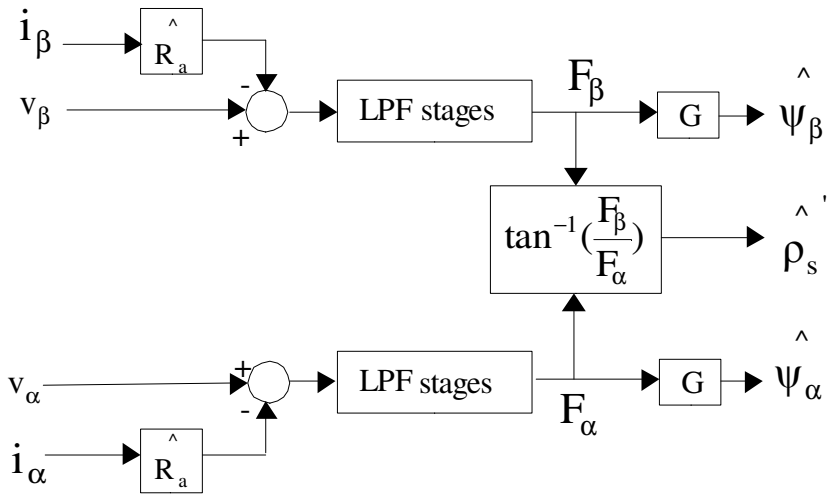

Fig 3.2 Estimator using MPCLPF

$$H(s) = G\left(\frac{1}{\tau s+1}\right)^n \tag{3-22}$$

And (3-21) is changed to (3-23) using (3-20).

$$G = \frac{1}{\omega_e}\sqrt{\left[1+\tan^2(\frac{\pi}{2n})\right]^n} \tag{3-23}$$

And finally gain is calculated as follows using (3-19).

$$G = \frac{1}{\omega_e}\left|\frac{1}{\cos(\frac{\pi}{2n})}\right|^n \tag{3-24}$$

The gain and consequently the effect of DC offset will be minimized when numerous LPF is used as shown in (3-25).

$$G_{min} = \lim_{n\to\infty}\frac{1}{\omega_e}\left|\frac{1}{\cos(\frac{\pi}{2n})}\right|^n = \frac{1}{\omega_e} \tag{3-25}$$

To study the affect of LPF stages on DC-offset, normalized transfer function is used. The Ratio of EPCLPF transfer function to its response at reference frequency which is defined as normalized transfer function is shown in (3-26).

$$\left|\frac{H(\omega)}{H(\omega_e)}\right| = \left|\frac{1}{\cos^2(\frac{\pi}{2n}) + (\frac{\omega}{\omega_e})^2 \sin^2(\frac{\pi}{2n})}\right|^{\frac{n}{2}} \qquad \text{For} \quad n > 1 \tag{3-26}$$

Derivative of (3-26) is shown in (3-27).

$$d\left|\frac{H(\omega)}{H(\omega_e)}\right| / dn = \frac{n}{2}\left|\cos^2(\frac{\pi}{2n}) + (\frac{\omega}{\omega_e})^2 \sin^2(\frac{\pi}{2n})\right|^{-(\frac{n}{2}+1)} \left(\cos(\frac{\pi}{2n})\sin(\frac{\pi}{2n})(\frac{\pi}{n^2})\right)\left((\frac{\omega}{\omega_e})^2 - 1\right) \tag{3-27}$$

In (3-27) the first and second terms are always more than zero, therefore (3-28) and (3-29) can be extracted.

$$\text{For } d\left|\frac{H(\omega)}{H(\omega_e)}\right| / dn > 0 \quad \left((\frac{\omega}{\omega_e})^2 - 1\right) > 0 \Longrightarrow (\frac{\omega}{\omega_e})^2 > 1 \Longrightarrow \omega_e < \omega \tag{3-28}$$

$$\text{For } d\left|\frac{H(\omega)}{H(\omega_e)}\right| / dn < 0 \quad \left((\frac{\omega}{\omega_e})^2 - 1\right) < 0 \Longrightarrow (\frac{\omega}{\omega_e})^2 < 1 \Longrightarrow \omega_e > \omega \tag{3-29}$$

And (3-28) and (3-29) can be written in form (3-30) and (3-31).

$$\text{For } \omega > \omega_e \quad d\left|\frac{H(\omega)}{H(\omega_e)}\right| / dn > 0 \tag{3-30}$$

$$\text{For } \omega < \omega_e \quad d\left|\frac{H(\omega)}{H(\omega_e)}\right| / dn < 0 \tag{3-31}$$

As seen in (3-31) for frequencies less than main supplying frequency (including DC offset and low frequency noise), the normalized transfer function decrease when filter stages increase thus the gain and consequently DC offset are reduced when several LPF with shorter time constant is used instead of few LPF with long time constant. And as shown in (3-32) the effect of DC offset is minimized when the filter stages approaches to ∞.

$$\text{Min}\left|\frac{H(0)}{H(\omega_e)}\right| = \lim_{n \to \infty}\left|\frac{1}{\cos(\frac{\pi}{2n})}\right|^n = 1 \tag{3-32}$$

Because the reference frequency is used in calculation of EPCLPF time constant, any error in speed estimation causes error in angle estimation. To study the effect of LPF stages on estimation

robustness or tolerance to speed estimation errors, the rate of normalized transfer function is calculated in (3-33).

$$d\left|\frac{H(\omega)}{H(\omega_e)}\right|/d\omega = -\frac{n}{2}\left|\cos^2(\frac{\pi}{2n}) + (\frac{\omega}{\omega_e})^2\sin^2(\frac{\pi}{2n})\right|^{-(\frac{n}{2}+1)} \frac{2\omega}{\omega_e^{\,2}}\sin^2(\frac{\pi}{2n}) \tag{3-33}$$

And limit of normalized transfer function rate, as frequency approaches to reference frequency is shown in (3-34).

$$\lim_{\omega \to \omega_e}\left(d\left|\frac{H(\omega)}{H(\omega_e)}\right|/d\omega\right) = -\frac{1}{\omega_e}K(n) \tag{3-34}$$

Where K(n) is coefficient function and is calculated in (3-35).

$$K(n) = n\sin^2(\frac{\pi}{2n}) \tag{3-35}$$

As seen in (3-34) because the frequency appears at denominator, the effect of error in low speeds increase. Therefore to reduce this error, coefficient function should be reduced. (3-35) shows the coefficient function is reduced when n increased. Thus to control motor in very low speed area K(n) should be reduce by increasing filter stages.

The limit of coefficient function and normalized transfer function as the filter stages approaches to ∞ is shown in (3-36) and (3-37) respectively.

$$\lim_{n \to \infty} K(n) = 0 \tag{3-36}$$

$$\lim_{n \to \infty}\left|\frac{H(\omega)}{H(\omega_e)}\right| = 1 \tag{3-37}$$

This equations show, in enough high n the output is not depended on reference frequency and tolerance to speed estimation errors increase by increasing n.

The simulation result using 3, 6,9,12 and 15 low pass filters for frequency 1Hz, which are shown in Fig 3.3, confirm that the effect of DC offset is reduced by extending the stages of low pas filters.

As seen in these results, although the phase angles of high stages LPF and low stages LPF are same, the effect of DC-offset in output is reduced effectively when high stages LPF is employed.

On the other hand, the slope of the 3 stages curve is more than 6 stages notably thus if some error is happen in speed calculation, the flux estimation error and consequently phase angle estimation error in low stages is more than high stages filters.

Because of these reasons the stages of filters is extended. However the use of large number of LPF is difficult because of the computation time and hardware limitation. In practical test it was

seen that the results of six or more stages are almost same, thus in this research a six stages LPF is used.

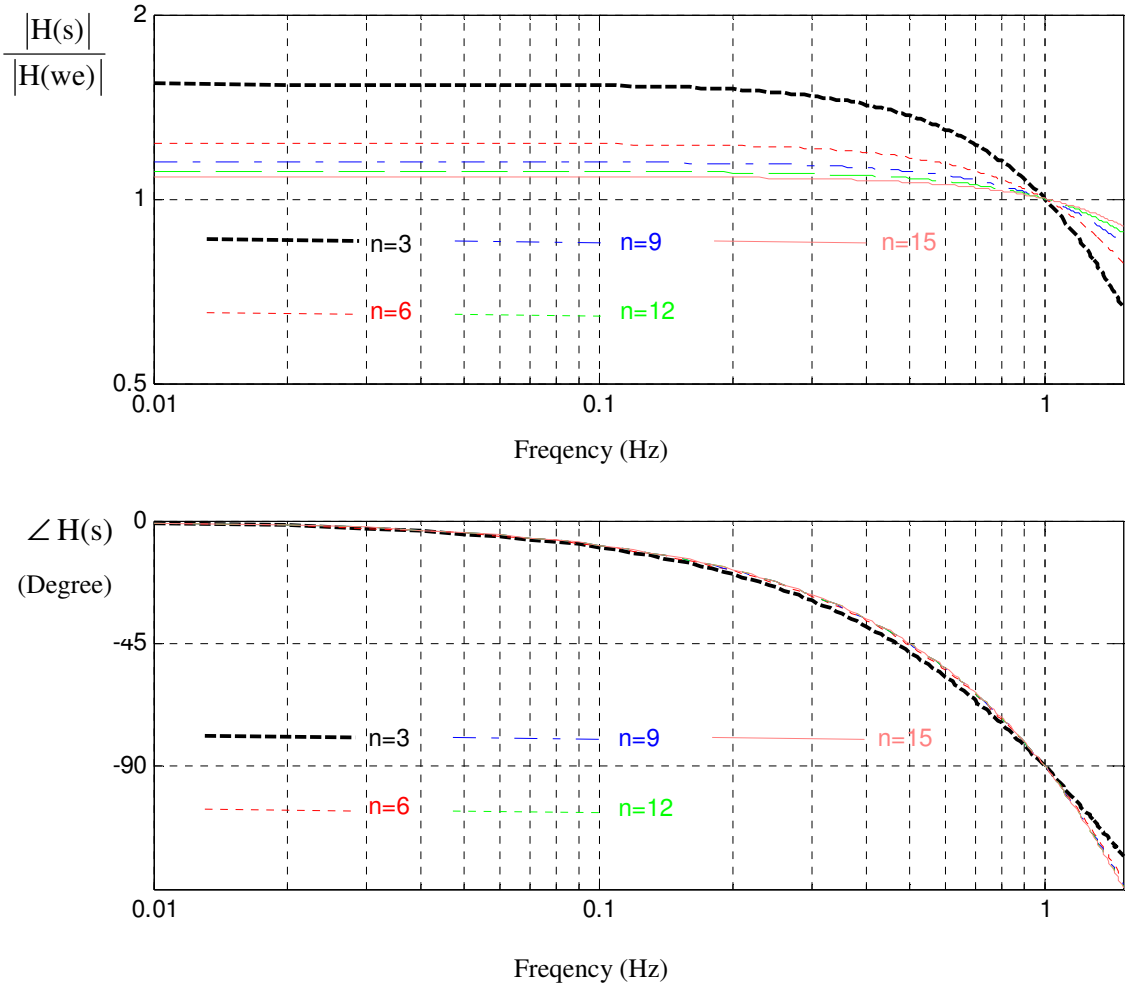

Fig. 3.3 The response for n stages cascaded filters for frequency 1Hz

In an extended PCLPF not only the stages of LPF are extended but also as a modified MPCLPF in phase angle calculation, gain is eliminated.

Thus for a 6 stages extended PCLPF the phase angle calculation is achieved using following equations.

$$H^{''}(s) = \left(\frac{1}{\tau s+1}\right)^{6} \tag{3-38}$$

$$F_{\alpha} = \left(v_{\alpha} - R_{a} i_{\alpha}\right) H^{''}(s) \tag{3-39}$$

$$F_{\beta} = \left(v_{\beta} - R_{a} i_{\beta}\right) H^{''}(s) \tag{3-40}$$

$$\hat{\rho}_s'' = \tan^{-1}\left(\frac{F_\beta}{F_\alpha}\right) \tag{3-41}$$

Where $H''(s)$ is defined as EPCLPF transfer function**.**

3.5.3 Calculation of rotor angle

To calculate rotor angle (θ_r), the vector diagram of the motor fluxes, as shown in Fig.3.4, is used.

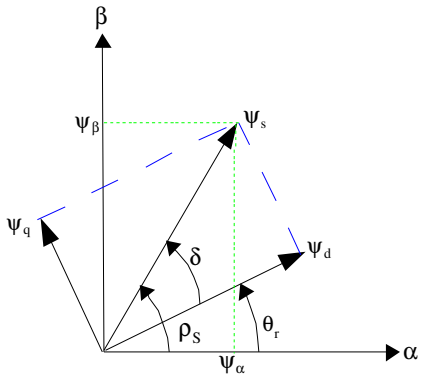

Fig. 3.4 Flux vector diagra

The relationship between θ_r, load angle (ρ_s) and δ, which is presented in (3-42), are extracted using this figure.

$$\theta_r = \rho_s - \delta \tag{3-42}$$

And also from Fig.3.4 (43)-(44) can be written.

$$\psi_d = |\psi_S|\cos\delta = L_d i_d \tag{3-43}$$

$$\psi_q = |\psi_S|\sin\delta = L_q i_q \tag{3-44}$$

Finally load angle can be extracted in (3-46) by considering (3-43)-(3-45) and Fig.3 .

$$i_s = \sqrt{i_\alpha^2 + i_\beta^2} \tag{3-45}$$

$$\delta = \sin^{-1}\left[\left[\frac{L_q^2 |i_s|^2 / |\psi_s|^2 - L_q^2 / L_d^2}{1 - L_q^2 / L_d^2}\right]^{\frac{1}{2}}\right] \tag{3-46}$$

Because is assumed almost invariable at constant loads and its variation rate is considered small compared to ρ_s. Motor speed (ω_r) is calculated using ρ_s as follows :

$$\omega_r = \frac{d}{dt}\theta_r \approx \frac{d}{dt}\rho_s \tag{3-47}$$

In the proposed method, rotor angle estimation is not directly dependent on the motor speed. Therefore, at low speeds the estimated and actual rotor positions are in agreement. It is possible to control the motor in a wide range of speeds and control is achieved at very low speeds, as well as high speeds.

3.6 Implementation of Digital LPF

The block diagram of a low pass filter is shown in figure 3.5.

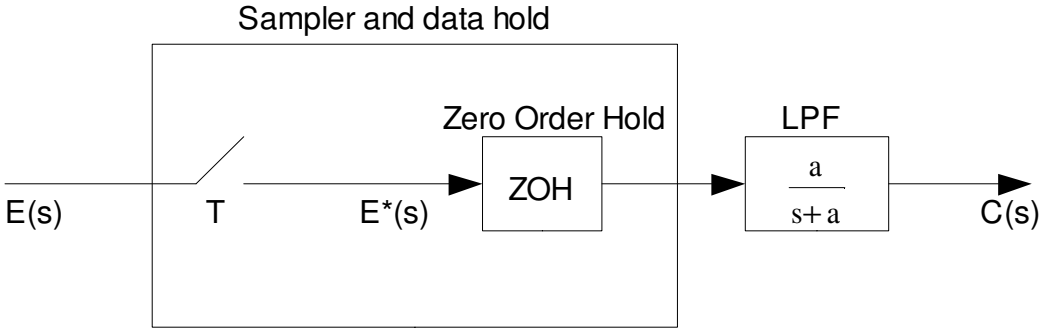

Fig. 3.5 Implementation of Digital LPF

Where $E(s)$ and $C(s)$ are defined as input and output and T is sampling period. Also $E^*(s)$ called the starred transform and is defined as (3-48).

$$E^*(s) = \sum_{n=0}^{\infty} e(nT)e^{-nTs} \tag{3-48}$$

Where $e(t)$ is input signal in time domain.

It is important to note that the definition of the sampling operation together with the zero-order-hold transfer function which is shown in figure 3.5 is defined as (3-49).

$$Z.O.H = \frac{1-e^{-Ts}}{s} \tag{3-49}$$

The transfer function of digital LPF which includes sample and holder is shown in (3-50).

$$A(s) = \frac{(1-e^{-Ts})a}{s(s+a)} = \left[\frac{a}{s(s+a)}\right]\left(1-e^{-Ts}\right) \tag{3-50}$$

This transfer function can be written as multiple of two function $B(s)$ and $B^*(s)$ as shown in (3-51)-(3-53)

$$B(s) = \frac{a}{s(s+a)} \tag{3-51}$$

$$F^{*}(s) = 1 - e^{-Ts} \tag{3-52}$$

$$A(s) = B(s)F^{*}(s) \tag{3-53}$$

The * shows that the $F^{*}(s)$ is a function of Ts.
The Z-transformation for (3-51) and (3-52) is presented in (3-54) and (3-55).

$$B(z) = \frac{z(1-e^{-aT})}{(z-1)(z-e^{-aT})} = \frac{(1-e^{-aT})}{(1-z^{-1})(z-e^{-aT})} \tag{3-54}$$

$$F(z) = 1 - z^{-1} \tag{3-55}$$

Thus (3-53) is transformed to (3-56).

$$A(z) = B(z)F(z) \tag{3-56}$$

Finally the transfer function of filter and sample and hold is defined as follows:

$$A(z) = \frac{(1-e^{-aT})}{(Z-e^{-aT})} \tag{3-57}$$

And the output signal is calculated as follows.

$$C(z) = A(z)E(z) \tag{3-58}$$

$$C(z) = \frac{(1-e^{-aT})}{(z-e^{-aT})}E(z) \tag{3-59}$$

$$C(z)(z-e^{-aT}) = (1-e^{-aT})E(z) \tag{3-60}$$

$$C(z)z - C(z)e^{-aT} = E(z) - E(z)e^{-aT} \tag{3-61}$$

(3-62) and (3-63) is extracted from z-transformation theorems.

$$Z\{c(k+n)\} = z^{-n}\left[C(z) - \sum_{k=0}^{n-1} c(k)Z^{-k}\right] \tag{3-62}$$

$$Z\{c(k-n)\} = z^{-n}C(z) \tag{3-63}$$

where Z is operator of Z-transform.
(3-61) is changed to (3-64) using inverse of z-transform which is shown by Z^{-1}.

$$Z^{-1}\{C(z)z\} - e^{-aT}Z^{-1}\{C(z)\} = Z^{-1}\{E(z)\} - e^{-aT}Z^{-1}\{E(z)\} \tag{3-64}$$

for n=1 (3-63) is transformed to (3-62).

$$Z\{c(k+1)\} = z\left[C(z) - \sum_{k=0}^{0} c(k)z^{-k}\right] = zC(z) \tag{3-65}$$

And finally,

$$c(k+1) = Z^{-1}\{zC(z)\} \tag{3-66}$$

And from (3-61) and (3-66), equation (3-67) is written.

$$c(k+1) - c(k)e^{-aT} = e(k) - e(k)e^{-aT} \tag{3-67}$$

And finally the digital LPF will be calculated as (3-68).

$$c(k+1) = e^{-aT}c(k) + (1 - e^{-aT})e(k) \tag{3-68}$$

Where c(k+1) and c(k) are the output in current and previous calculation steps respectively.

3.7 conclusions

Although using fundamental models to estimate angles is the most straightforward approach and has several advantages, immunity to noise, offset and drift should be achieved using appropriate techniques else measurement noise and DC offset causes an increasing error in the estimator.

Use of programmable cascaded low pass filters (PCLPF) instead of pure integrators is alternative method to reduce drift-error and it has previously been applied to the sensorless control of induction motors. In this chapter, this filter is adapted to estimate phase angle at low speed and near zero speed area in SYRM. To estimate rotor angle at low speed, modified programmable cascaded low pass filter (MPCLF) is presented by authors. The problems of PCLPF are reduced because the PCLPF gain is eliminated in phase angle calculation.

In the next stage, the range of rotor angle calculation is expanded from near zero speed to high speed by proposing extended programmable cascaded low pass filters (EPCPLF). The performance of these filters is improved considerably by extending their stages and reduces its gain. Because the proposed method reduces the PCLPF drawbacks at low speed, effectively, the rotor angle estimation at very low speed is valid and thus, sensorless control at near zero speed is possible.

Although the rotor angle estimation using EPCPLF is possible at near zero speed, but more calculation time is needed compared with MPCLPF. Thus we suggest using EPCLPF in very low speed precise application while MPCPLF can be used in low speed application when there is limitation in hardware capacity.

Chapter 4

Online parameter identification using block pulse function

4.1 Summary

In this chapter the effect of the parameter variation on sensorless vector control and its compensation method are considered. At first the effect of stator resistance variations in phase angle calculation is explained and its effect in low speed is surveyed. The inductance importance in load angle estimation and decoupling signals is shown. Our proposed identification is presented. And block pulse function is introduced. Then the equations of proposed parameter identification method are discussed and it is shown that this method is not affected by position estimation accuracy. Finally the chapter conclusion is explained.

4.2 Variation of armature parameters at low speed

In rotor angle calculation using estimated stator flux linkage, as seen in equations (3-1)-(3-2), the rotor angle estimation is dependent on armature inductance and armature resistance. Thus, any variation in motor parameters will disorder position estimation.

The effect of stator resistance variation is more important in low speed regions, because as the stator frequency reduces at lower speed, the inverter voltage magnitude decreases in relation to stator resistance voltage and the resistance voltage dominates the integrator input in low speed [5]-[7]. Thus particularly the stator resistance determines the estimation accuracy of the stator flux vector in low speed. Conversely, it has little effect on the integrator input at higher speed as the nominal value of $R_a i_\alpha$ is low.

Because the resistance of the winding material increases with temperature and can vary in a 1:2 range, considerable variations of the stator resistance take place when the machine temperature changes at varying load. These need to be tracked to maintain the system stability at low speed.

On the other hand, as there is no permanent magnet in SYRM, the motor current includes magnetizing and torque components. Therefore the motor current is pretty high especially at high loads. And this leads to saturation of motor inductance. And because the motor inductance is very important in calculation of load angle and decoupling signals, they should be defined precisely else the vector control will be not valid.

An observer constructed from the machine model can be used for parameter estimation. Although as a thermal effect, variations of the stator resistance occur slowly, the identification scheme for the stator resistance must be fast because the effect of saturation. A fast command to lower speed leaves this parameter incorrectly tuned, unless it gets identified as soon as the sensitivity of the estimation algorithm returns.

In addition, to avoid using voltage transducers, the actual voltage is not measured and the reference voltage is used in the phase angle estimation. However, the nonlinearity of the PWM inverter, caused by dead-time effect, on-state voltage drop and threshold voltage of the power semiconductor switches, make the machine terminal voltages different from reference voltages when motor speed and the amplitudes of the stator voltages are low [5]-[6], [39], [45].

Since rotor angle estimation is main aim, armature resistance and nonlinearity of the inverter having the same effect on rotor angle estimation, the effect of these nonlinearities can be compensated, by assuming it as an additional nonlinear resistance series with armature. Therefore the identified resistance includes armature resistance and the effect of power switch nonlinearity. For proper rotor angle estimation this resistance should be identified during motor operation.

In this thesis to avoid parameter variation drawbacks an online parameter identification method which does not depend on estimation accuracy is suggested [43], [45]. In the proposed method, motor parameter identification is done using a block pulse function (BPF) instead of the Euler method which is used in [35]-[37]. The BPF increases calculation precision while its computation time is almost the same as the Euler algorithm [46], [47].

4.3 System Identification using block pulse function

The Block Pulse Functions (BPF) is a set of orthogonal functions with piecewise constant values and to use the BPF approximation, differential equations are transformed approximately into their corresponding algebraic forms based on the operation rules of BPF, so that the numerical solutions obtained more directly. And it increases calculation precision compared with the Euler method [46], [47].

The BPF analysis is suitable when the input and output of the system is obtained as average values because the approximations by BPF are based on the average values.

Also we can use the derived relation between the inputs and the state in block pulse regression to estimate the unknown parameter matrices.

The definition of BPF is shown in (4-1)-(4-2).

$$\phi_i(t) = \begin{cases} 1 \text{ for } (i-1)\dfrac{T}{m} \le t \le \dfrac{iT}{m} \\ 0 \text{ otherwise} \end{cases} \tag{4-1}$$

$$\Phi(t) = [\phi_1(t) \ \phi_2(t) \ .....\phi_i(t) \ .....\phi_m(t)] \tag{4-2}$$

Where m is an arbitrary positive integer and T is the final time.

(4-3) shows the integral of BPF which is defined by P.

$$\int \Phi(t)dt = P\Phi(t) \tag{4-3}$$

And from P is calculated as a $m \times m$ matrix shown in (4-4).

$$P = \frac{h}{2}\begin{bmatrix} 1\,2\,2\ldots\ldots\ldots\ldots 2\,2\,2 \\ 0\,1\,2\ldots\ldots\ldots\ldots 2\,2\,2 \\ 0\,0\,1\ldots\ldots\ldots\ldots 2\,2\,2 \\ \ldots\ldots\ldots\ldots\ldots\ldots\ldots \\ 0\,0\,0\ldots\ldots\ldots\ldots 1\,2\,2 \\ 0\,0\,0\ldots\ldots\ldots\ldots 0\,1\,2 \\ 0\,0\,0\ldots\ldots\ldots\ldots 0\,0\,1 \end{bmatrix} \tag{4-4}$$

Where h is width of the block pulses and is defined as h = T/m.

To estimate the unknown parameter of a system using the BPF, its space states which shown in (4-3) should be expanded into a block pulse series.

$$\dot{X}(t) = AX(t) + BU(t) \tag{4-5}$$

Where $X(t)$, $U(t)$ are a matrix of input, a matrix of state and A and B are defined as system parameter matrix.

And the space state (4-5) transform approximately into its corresponding BPF algebraic forms shown (4-8) using (4-6) and (4-7).

$$X(t) \approx [x_1 \ x_2 \ .....x_k \ .....x_m]\Phi(t) = X\Phi(t) \tag{4-6}$$

$$U(t) \approx [u_1 \ u_2 \ .....u_k \ .....u_m]\Phi(t) = U\Phi(t) \tag{4-7}$$

$$(x_1 \ x_2 .....x_m)\Phi(t) - (x(0) \quad x(0) \ .....x(0) \ )\Phi(t) = A(x_1 \ x_2 .....x_m)P\Phi(t) + B(u_1 \ u_2 .....u_m)P\Phi(t) \tag{4-8}$$

Where x_k and u_k are the average values of input and state matrixes over the sampling period respectively.

The equation (4-8) is solved as follow.

$$x_k = \Gamma\left(x_k + \frac{h}{2} B u_k + h \sum_{j=1}^{k-1} (A x_j + B u_j) \right) \tag{4-9}$$

$$\Gamma = \left(I - \frac{h}{2} A \right)^{-1} \tag{4-10}$$

Where **I** is the unit matrix.

Although it is possible to calculate A and B directly from (4-9), its computation size is very large and this computations need a huge memory. Thus to estimate unknown parameter matrices, the relation between the inputs and states are derived in block pulse regression equation as shown in (4-11) and (4-12).

$$x_1 = \Gamma\left(x_0 + \frac{h}{2} B u_1 \right) \tag{4-11}$$

$$x_{k+1} = \Gamma\left(\left(I + \frac{h}{2} A \right) x_k + \frac{h}{2} B\left(u_{k+1} + u_k\right) \right) \tag{4-12}$$

Then the following equation using block pulse approximation can be obtained from (4-5).

$$x_{k+1} - x_k = \frac{h}{2}(A x_{k+1} + x_k) + \frac{h}{2} B (u_{k+1} + u_k) \tag{4-13}$$

All the (m-1) equations in (4-13) can be expressed in a matrix form as follows.

$$\theta^T = (A \; B) \tag{4-14}$$

$$G^T = \frac{h}{2} \begin{pmatrix} x_{k+1} + x_k \\ u_{k+1} + u_k \end{pmatrix} \tag{4-15}$$

$$F^T = \left[x_{k+1} - x_k \right] \tag{4-16}$$

$$F = G\theta \tag{4-17}$$

And finally the system parameter matrixes are identified using (4-18).

$$\theta = (G^T G)^{-1} G^T F \tag{4-18}$$

4.4 Sensor less parameter identification using block pulse function

When the data of the sensor is available, the parameter calculation can be done based on exact information of rotor angle. Conversely in the sensorless control the data of rotor angle is achieved using estimator instead of encoder. While the rotor angle estimation which is based on EPCLPF presented in chapter 3 can be done with high precision, there is a difference between actual and estimated rotating reference frame especially at low speed when the effects of noise and DC-offset is not negligible. Thus the identification method should not be affected by difference between

estimation and actual reference frame. In this thesis, the identification method is not depended on estimation accuracy.

To identify the parameters in sensorless control, the circuit equation of the SYRM in actual d-q coordinate , which is represented in equation (4-19), will be transformed to an estimated rotating coordinate, which is defined here as $\delta - \gamma$, using (4-20) and (4-21).

$$\begin{bmatrix} v_d \\ v_q \end{bmatrix} = \begin{bmatrix} R_a + PL_d & -\omega_r L_q \\ \omega_r L_d & R_a + PL_q \end{bmatrix} \begin{bmatrix} i_d \\ i_q \end{bmatrix} \tag{4-19}$$

$$\begin{bmatrix} v_\gamma \\ v_\delta \end{bmatrix} = \begin{bmatrix} \cos\Delta\theta & -\sin\Delta\theta \\ \sin\Delta\theta & \cos\Delta\theta \end{bmatrix} \begin{bmatrix} v_d \\ v_q \end{bmatrix} \tag{4-20}$$

$$\begin{bmatrix} i_\gamma \\ i_\delta \end{bmatrix} = \begin{bmatrix} \cos\Delta\theta & -\sin\Delta\theta \\ \sin\Delta\theta & \cos\Delta\theta \end{bmatrix} \begin{bmatrix} i_d \\ i_q \end{bmatrix} \tag{4-21}$$

Where $\Delta\theta$ is the angle difference of actual d-q axes and the estimated $\delta - \gamma$ axes which is shown in Fig. 4.1.

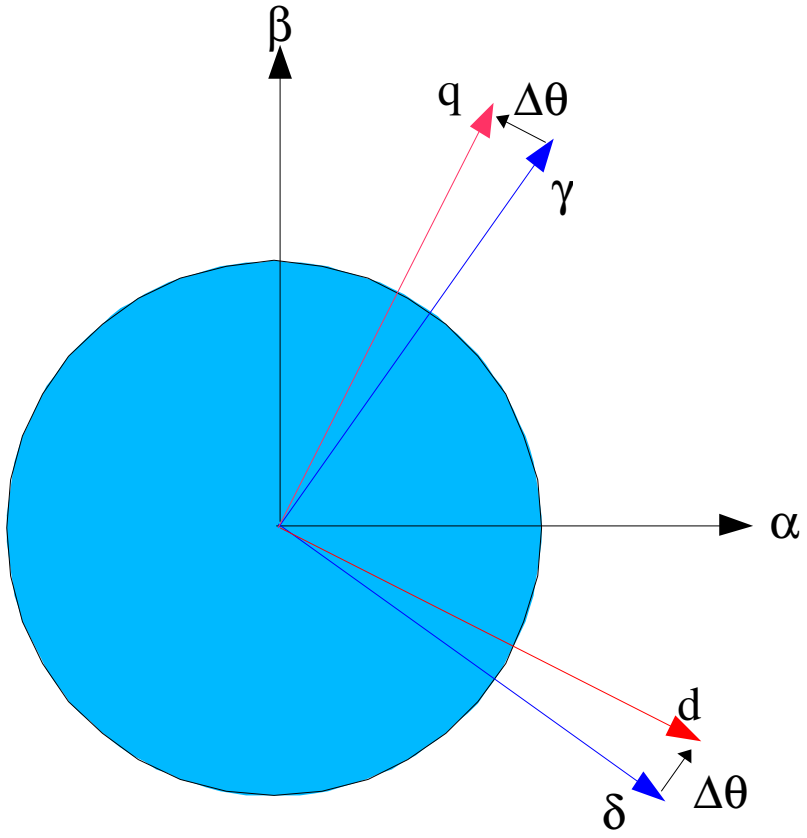

Fig. 4.1 Estimated and actual rotating coordinates

The space state form of the SYRM which includes motor parameter matrices is extracted in (4-22). And the equations of parameter matrices, which are defined as A and B, and motor parameters are shown in (4-23)-(4-28).

$$\frac{d}{dt}\begin{bmatrix} i_\gamma \\ i_\delta \end{bmatrix} = A\begin{bmatrix} i_\gamma \\ i_\delta \end{bmatrix} + B\begin{bmatrix} v_\gamma \\ v_\delta \end{bmatrix} \tag{4-22}$$

$$A = \begin{bmatrix} a_{11} & a_{12} \\ a_{21} & a_{22} \end{bmatrix} = \frac{-R_a(L_d + L_q)}{2L_dL_q}\begin{bmatrix} 1 & 0 \\ 0 & 1 \end{bmatrix} + \frac{R_a(L_d - L_q)}{2L_dL_q}\begin{bmatrix} \cos 2\Delta\theta & \sin 2\Delta\theta \\ \sin 2\Delta\theta & -\cos 2\Delta\theta \end{bmatrix} \tag{4-23}$$
$$+ \frac{\omega_{re}}{L_dL_q}\begin{bmatrix} M_{11} & M_{12} \\ M_{21} & M_{22} \end{bmatrix}$$

$$B = \begin{bmatrix} b_{11} & b_{12} \\ b_{21} & b_{22} \end{bmatrix} = \frac{(L_d + L_q)}{2L_dL_q}\begin{bmatrix} 1 & 0 \\ 0 & 1 \end{bmatrix} - \frac{(L_d - L_q)}{2L_dL_q}\begin{bmatrix} \cos 2\Delta\theta & \sin 2\Delta\theta \\ \sin 2\Delta\theta & -\cos 2\Delta\theta \end{bmatrix} \tag{4-24}$$

$$M_{11} = \frac{1}{2}\sin 2\Delta\theta\,(L_d^2 - L_q^2) \tag{4-25}$$

$$M_{12} = \frac{1}{2}\left[(L_d^2 + L_q^2) + \cos 2\Delta\theta\,(L_d^2 - L_q^2)\right] \tag{4-26}$$

$$M_{21} = -\frac{1}{2}\left[(L_d^2 + L_q^2) + \cos 2\Delta\theta\,(L_d^2 - L_q^2)\right] \tag{4-27}$$

$$M_{22} = -\frac{1}{2}\sin 2\Delta\theta\,(L_d^2 - L_q^2) \tag{4-28}$$

To identify the motor parameter matrix, phase currents are defined as input matrix, while the voltages are an output matrix in equations (4-28) and (4-29). As mentioned previously, the direct computations need a large memory size thus it should be solved recursively using BPF, as shown in (4-31)-(4-32).

$$U = \begin{bmatrix} v_\gamma & v_\delta \end{bmatrix}^T \tag{4-29}$$

$$X = \begin{bmatrix} i_\gamma & i_\delta \end{bmatrix}^T \tag{4-30}$$

$$X_{k+1} = \Gamma\left(\left(I + \frac{h}{2}A\right)X_k + \frac{h}{2}B(U_{k+1} + U_k)\right) \tag{4-31}$$

$$\Gamma = \left(I - \frac{h}{2}A\right)^{-1} \tag{4-32}$$

Where **I** is the unit matrix.

Thus the motor state equation shown in (4-22) is transformed approximately into its BPF corresponding algebraic forms, which are shown in (4-33).

$$\begin{bmatrix} i_{\gamma(k+1)} - i_{\gamma(k)} \\ i_{\delta(k+1)} - i_{\delta(k)} \end{bmatrix} = \frac{h}{2} A \begin{bmatrix} i_{\gamma(k+1)} + i_{\gamma(k)} \\ i_{\delta(k+1)} + i_{\delta(k)} \end{bmatrix} + \frac{h}{2} B \begin{bmatrix} v_{\gamma(k+1)} + v_{\gamma(k)} \\ v_{\delta(k+1)} + v_{\delta(k)} \end{bmatrix} \tag{4-33}$$

Equation (33) is a derived relation between the voltages and currents in a block pulse regression equation. And matrix of θ includes A and B, are calculated using (4-14)-(4-18). The unknown parameter matrices θ can be estimated using recursive least square (RLS) algorithm [61], which reduces computation size efficiently, as shown in follows.

$$g_k = \frac{h}{2} \begin{pmatrix} x_{k+1} + x_k \\ u_{k+1} + u_k \end{pmatrix} \tag{4-34}$$

$$f_k^T = x_{k+1} - x_k \tag{4-35}$$

$$\theta_k = \theta_{k-1} + \zeta_k S_{k-1} g_k (f_k - g_k^T \theta_{k-1}) \tag{4-36}$$

$$S_k = (S_{k-1} - \zeta_k S_{k-1} g_k g_k^T S_{k-1}) \tag{4-37}$$

$$\zeta_k = \frac{1}{\alpha + g_k^T S_{k-1} g_k} \tag{4-38}$$

$$S_0 = c^2 I \tag{4-39}$$

$$\theta_0 = 0 \tag{4-40}$$

Where α is defined as forgetting factor and $0 < \alpha \leq 1$. And the value of c should sufficiently be large.

To calculate motor parameter, the following equations are used [35]-[37].

$$M_1 = a_{11} + a_{22} = \frac{L_d + L_d}{L_d L_q} \tag{4-41}$$

$$M_2 = b_{11} + b_{22} = \frac{-R_a(L_d + L_d)}{L_d L_q} \tag{4-42}$$

$$M_3 = \sqrt{(b_{11} - b_{22})^2 + 4b_{12}b_{21}} = \frac{-(L_d - L_d)}{L_d L_q} \tag{4-43}$$

$$L_d = \frac{2}{M_1 - M_3} \tag{4-44}$$

$$L_q = \frac{2}{M_1 + M_3} \tag{4-45}$$

As shown in equations (4-41)-(4-45) although parameter matrixes (A, B) include $\Delta\theta$, the identified parameter is not dependent on $\Delta\theta$. Hence, in this method, parameter identification is not affected by position estimation accuracy [35]-[37].

4.5 Conclusion

In open loop fundamental models which was explained in chapter 1, stator resistance and inductances must be defined precisely else the rotor angle estimation is not valid. The stator resistance is important at phase angle calculation especially in low speeds while the motor inductances are required for load angle estimation. Thus a proper method for identifying motor parameter is essential. On the other hand this identified parameter is used in calculation of decoupling signals. Also the nonlinearity of inverter should be considered in reference voltage calculation.

In this chapter an online parameter identification method which does not depend on estimation accuracy is proposed. In the proposed method, motor parameter identification is done using a block pulse function (BPF) instead of the Euler method which is used in pervious researches. It saves calculation time compared with the other numerical analysis method.

It is shown although the identified parameter is not dependent on angle difference of actual d-q axes and the estimated $\delta - \gamma$ axes. Hence, in this method, parameter identification is not affected by position estimation accuracy.

Chapter 5

Proposed sensorless speed vector control

5.1 Summary

In this chapter the proposed sensorless vector control is presented and its block diagram is explained. And it is shown that MPCLPF and EPCLPF and online parameter identification that are explained in previous chapters are employed in this block diagram. To startup motor in stand still condition a novel method which uses EPCLPF is suggested. The block diagram of proposed method is presented and its operation is explained.

The block diagram of practical system configuration is presented and the proposed experimental setup is presented and its hardware and software is discussed. Then the practical result of sensorless control and proposed parameter identification is presented.

The result of MPCLPF estimator, which was explained in chapter 3, in a wide range of speed is experienced and its stability is tested by adding an artificial DC-offset to measured currents. The transient response of proposed method is presented and the result of two close loop control strategy is shown.

The effect of EPCLPF which includes 6 stages LPF filter is presented in low speed and very low speed area. And it is shown that estimation is achieved even near zero speed. The step responses of reference speed and torque load are evaluated, and the result of direction changed is investigated.

The result of motor start up ability is presented in this chapter. And finally the effect of stages of low pass filters on DC-offset problems is studied.

5.2 Speed sensorless control of SYRM

The block diagram of the proposed sensorless control method is shown in Fig. 5.1.

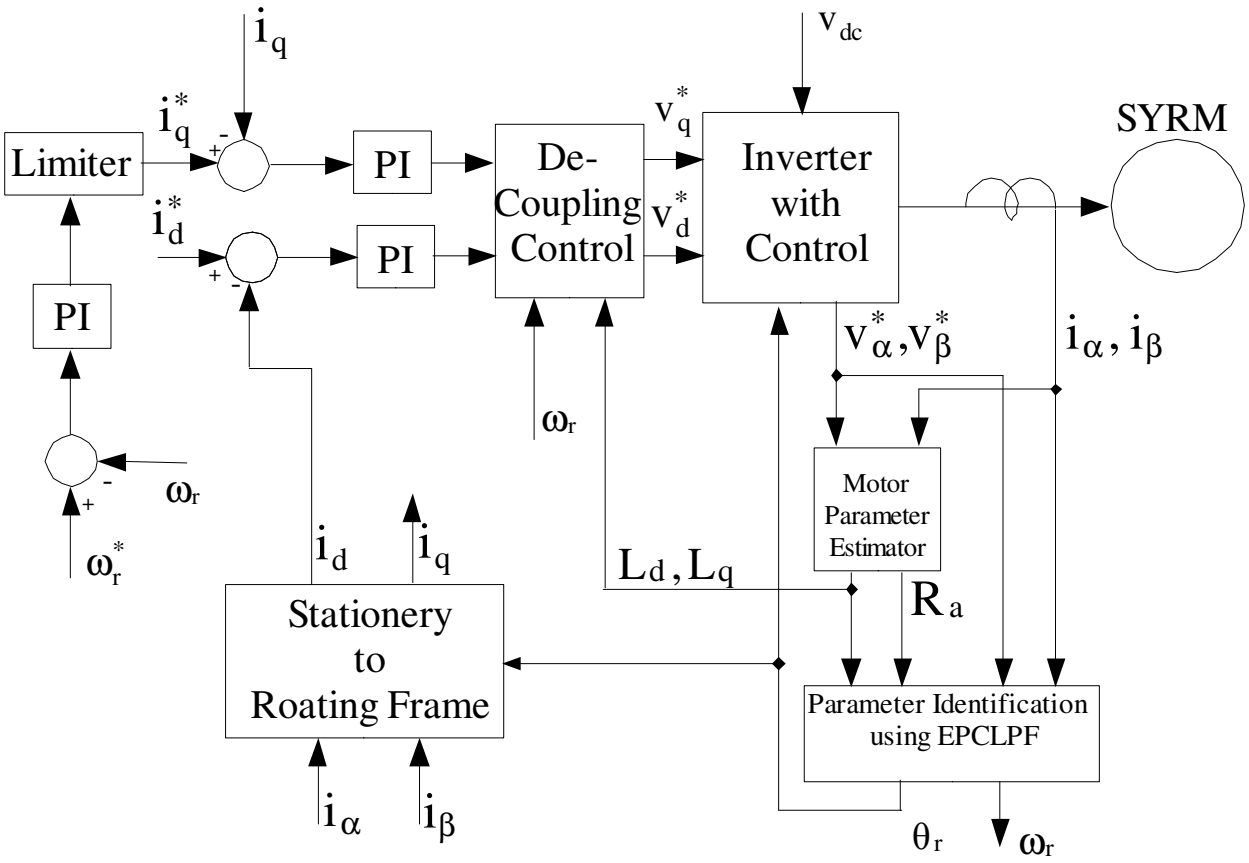

Fig. 5.1 The block diagram of sensorless vector control of SYRM

Where ρ_s, ω_r, ω_r^*, i_α and i_β are estimated rotor angle, estimated rotor speed, reference rotor speed and armature currents in a stationary reference frame respectively. Also v_d^*, v_q^*, i_d^* and i_q^* are references and i_d, i_q are estimated values in a rotating reference frame respectively. L_d, L_q and R_a are the motor parameters. Here i_q^* is defined by ω_r^* and i_d^* are regulated based on control strategies that are classified by a constant d-axis current, maximum torque per ampere ($i_d^* = i_q^*$) and maximum power factor control $(i_d^* = i_q^* \sqrt{\frac{L_q}{L_d}})$ [6]-[7]. The identified stator parameters are used in rotor angle and speed estimation, flux decoupling and i_d^* regulation.

5.3 Start up ability

The start up of SYRM has been a challenge for a long time. Because there is no current and voltage in motor the rotor angle estimation using voltages and current is not possible.

To solve this problem in our method as shown in figure 5.2, at the standstill condition, the rotor angle is assumed rotating at reference speed, and because the proposed EPCLPF can estimate rotor

angle at very low speed area, the estimated and actual rotor angle converge rapidly and the motor startup is done without the torque jerk caused by transition from the standstill mode to the vector control mode which usually is used in sensorless control of SYRM.

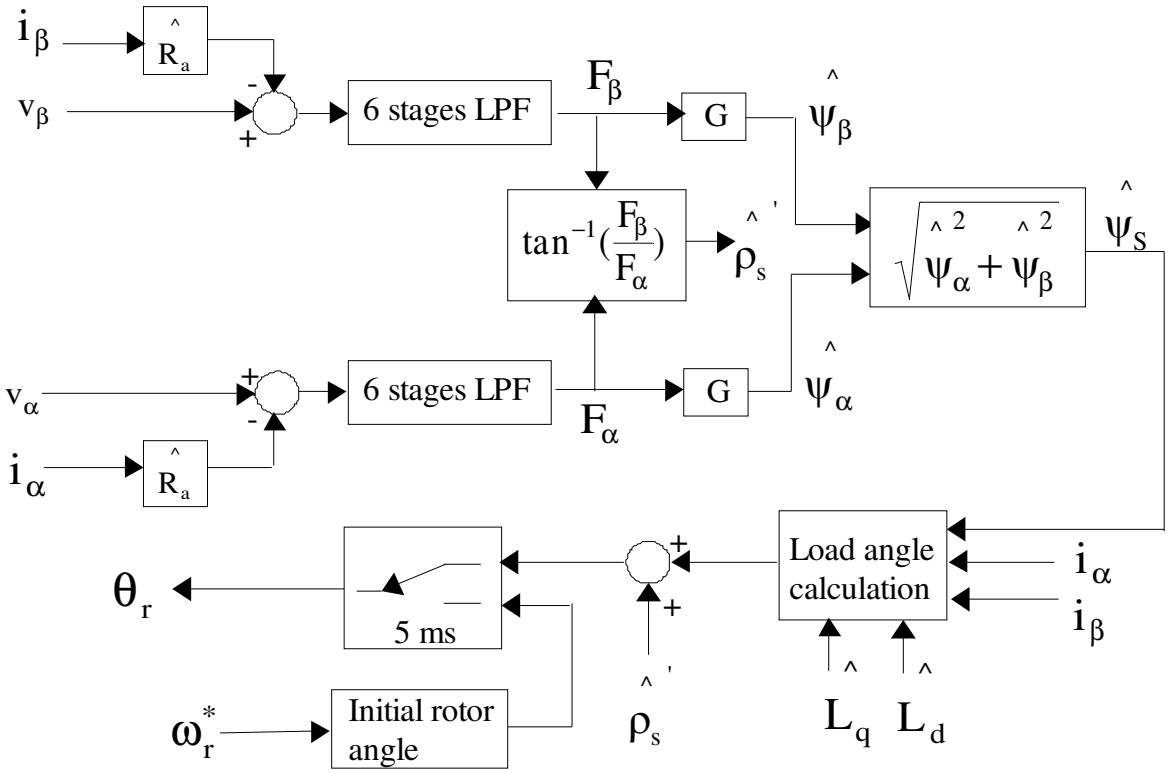

Fig. 5.2 Proposed estimation method

5.4 Experimental setup

To realize the validity of the control theory a PC-based control system is used in the experimental setup. Since, there is need for an appropriate operating system with real time control ability, the Real Time Linux (RTLinux) is used in this system. The RTLinux is a hard real-time operating system that handles time-critical tasks and runs the normal Linux as its lowest priority execution thread [62].

The experimental setup, which employs RTiC-Lab, includes a graphic user interface, remote monitoring and networking [63]. Therefore it is possible to monitor motor variables and change its reference variables or its control method strategy instantaneously during motor operation. This system consists of a Complex Programmable Logic Device (CPLD), 10MHz system clock and A/D converter. An ALTERA FLEX10K50 [64] is selected for CPLD device and the circuit is designed using VHDL. The speed and position detectors with speed correction function, clock the generator for the A/D converter and the ISA interface circuit are designed in it.

Fig.5.3 and Fig.5.4 show the RTLinux-based experimental system. As seen in Fig.5.3 currents

FPGA-Based Interface Board

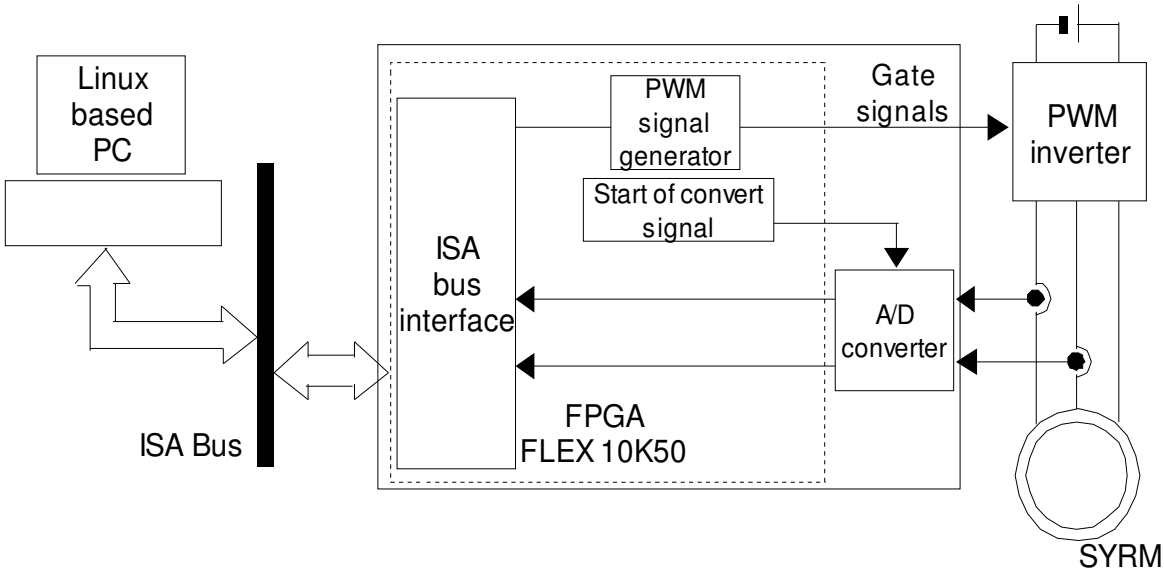

Fig.5.3 Configuration of the system

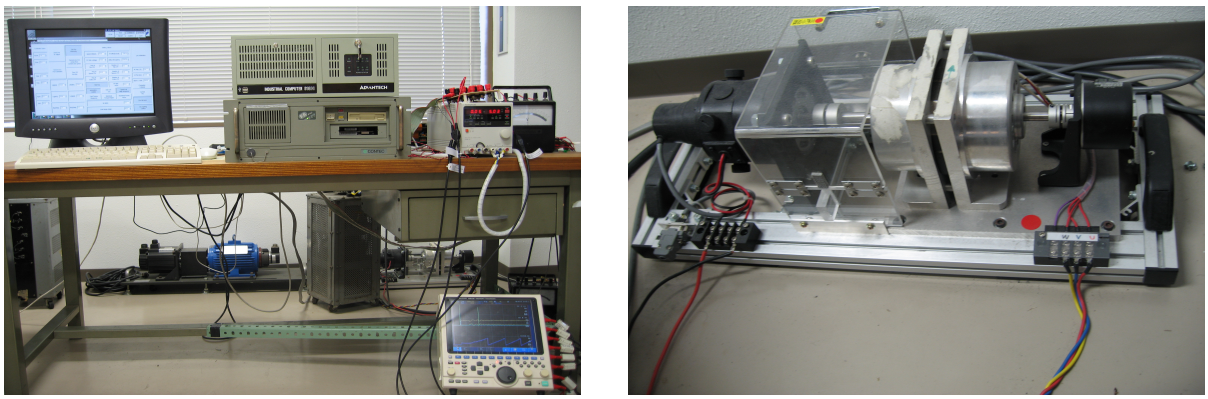

Fig. 5.4 Experimental Setup

Table 1. SYRM Motor Nominal Parameters

Rated Power	86W
Rated Torque	0.4 Nm
Rated Current	1.7A rms
d Axis Armature inductance	93 mH
q Axis Armature Inductance	36 mH
Armature Resistance	1.89 Ω
DC link Voltage	150 V
Pole	4

are sampled by A/D converter and link to the PC via the FPGA. The PWM inverter is driven by gate signals which are made by the PWM signal generator. The PC system is connected to the FPGA using the ISA Bus. The nominal parameter of the SYRM is shown in the Table 1.

5.5 Experimental results

5.5.1 Experimental results for parameter identification

Fig. 5.5 and Fig. 5.6 show the identified parameter in 100rpm and 600rpm respectively. As seen in this figures, there is a different between estimated parameter (especially resistance) in low and high speeds.

To illustrate this phenomenon it should be noted that in this paper the reference voltage is used instead of actual voltage. But the effects of inverter nonlinearity (include of dead-time effect, the on-state voltage drop and threshold voltage of semiconductor switches) cause a difference between reference and terminal voltages. This difference will be increase when the motor speed, and thereupon, stator voltage is low. Because this effect is important for accuracy of rotor angle estimation, this effect should be compensated. To compensate this error, the effect of inverter nonlinearity is assumed as a nonlinear resistance series with armature resistance. Thus the identified resistance includes armature resistance and the effect of power switches nonlinearity. Therefore because the effect of inverter nonlinearity, which is considered as additional nonlinear resistance series with armature circuit, increases in low speed, identified resistance in 100 rpm is grater than the case of 600 rpm.

On the other hand, the experimental results show, even with discrepancy between identified and rated resistance, rotor angle and motor speed estimations are valid. Because the identified resistance includes the effect of inverter nonlinearity it can compensate the difference between reference and machine terminal voltages caused of inverter nonlinearity. Actually the identified resistance shows the system resistance instead of armature resistance. And therefore rotor angle estimation is valid because the first part of this resistance expresses the effect of inverter nonlinearity.

In some papers to calculate inverter nonlinearity a model of inverter with parameter identification is used. But in our system, motor could operate satisfactorily using aforementioned method.

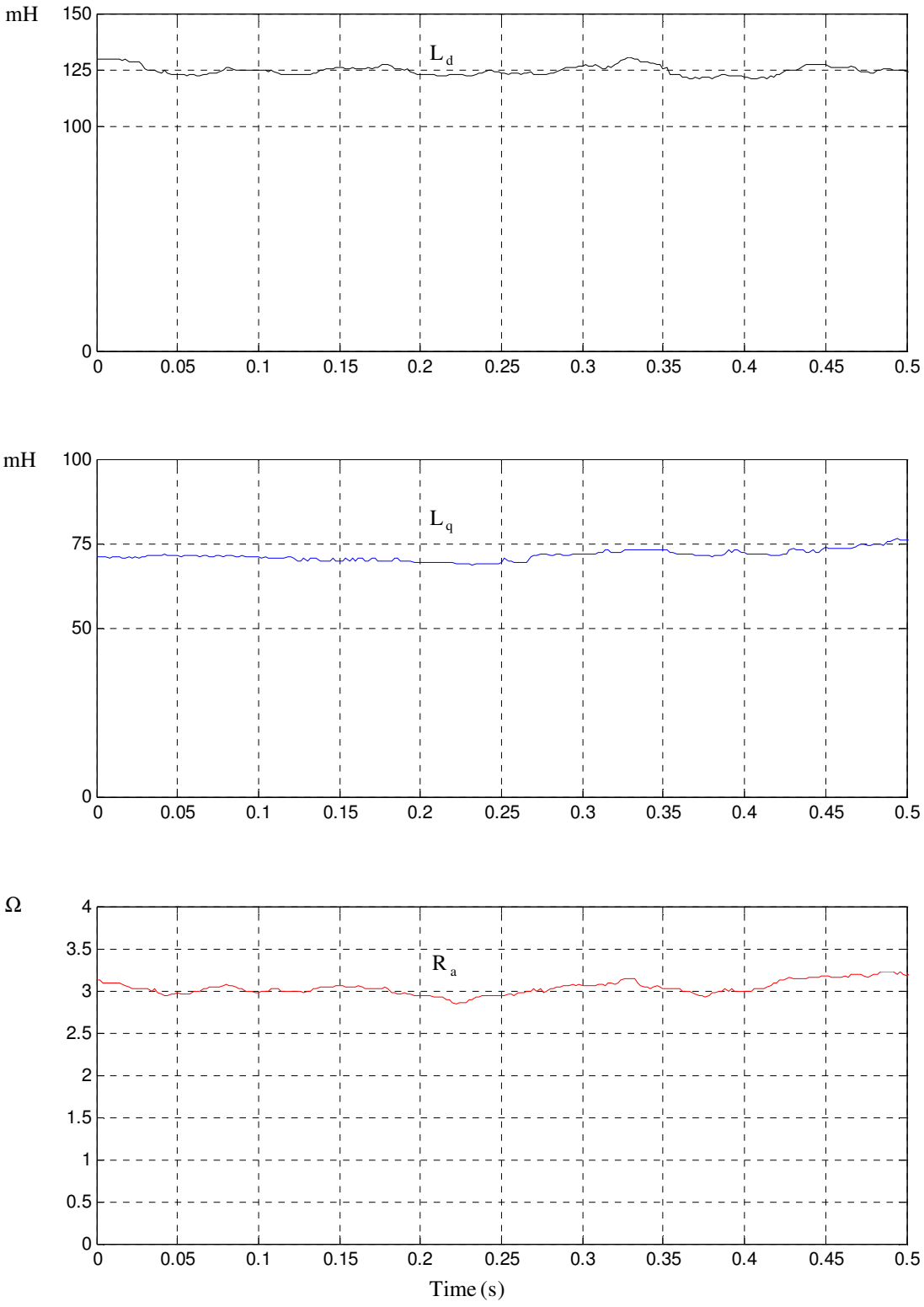

Fig. 5.5 Identified motor parameters at 100 rpm

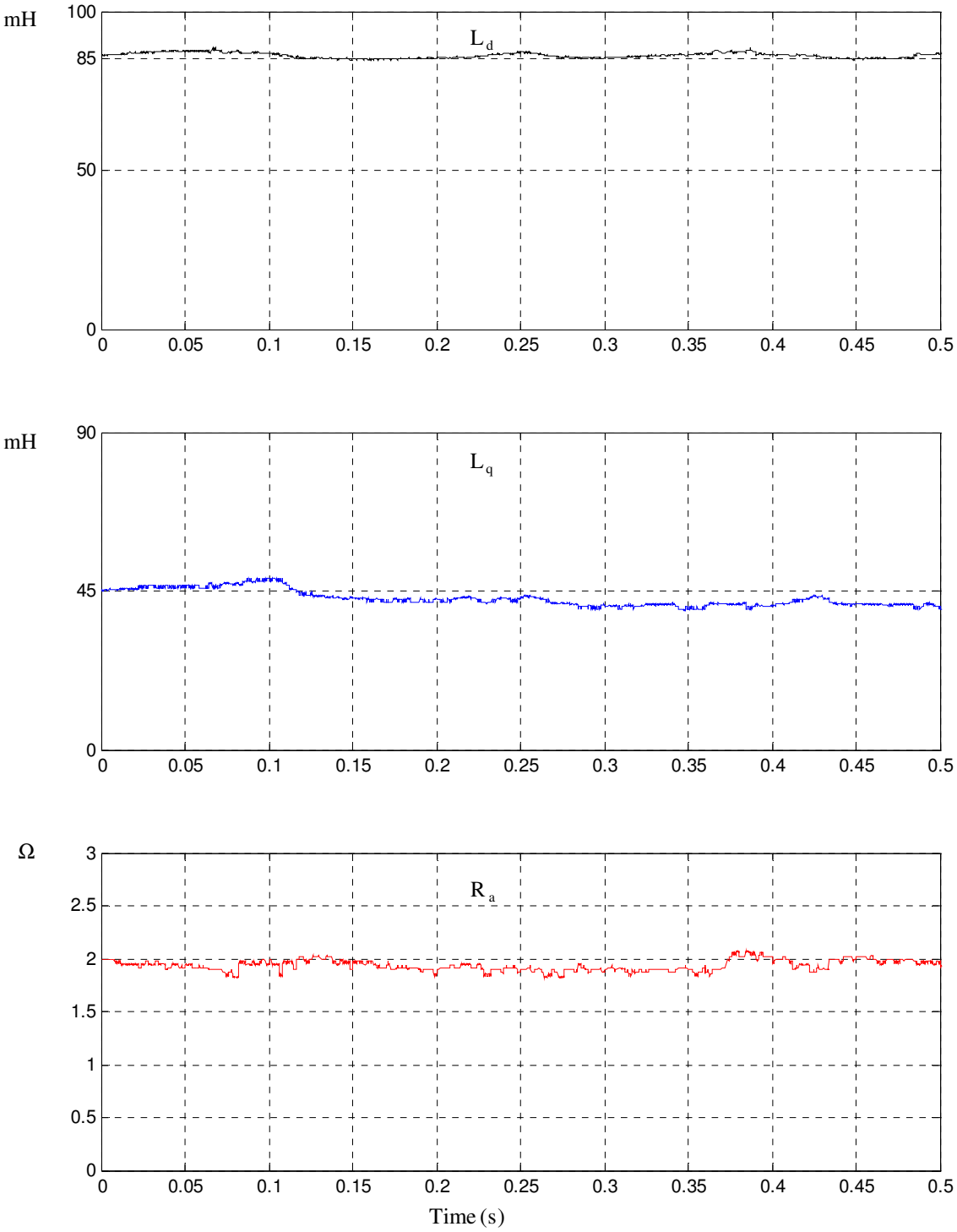

Fig. 5.6 Identified motor parameters at 600 rpm

5.5.2 Experimental results using MPCLPF

The experimental results using MPCLPF which are obtained at 100 rpm, 600 rpm and 1200 rpm are shown in Fig. (5-7)- (5-10). These results show that sensorless vector control is achieved at low speed regions, as well as, at high speeds using the proposed method.

Also, as seen in Fig. 5.7 and Fig. 5.9, the estimated rotor angle agrees with the actual rotor angle and the accuracy of the angle estimation, is acceptable at high and low speeds.

In practical experiments it was seen that even near 30~40 rpm the accuracy of rotor angle and speed estimation is acceptable and motor behavior is almost stable. Although at the speeds around 10 rpm sensorless control is achieved, the rotor angle estimation is not accurate (there is a considerable difference between actual and estimated rotor angle at 10 rpm). Therefore 30~40 rpm (about 1.5~2 percent of nominal speed) is minimum speed that rotor angle estimation is acceptable.

To test the estimation robustness again the DC offset, 25 mA was added to the motor current signals while the motor was operating at 20% of rated torque, and as shown in Fig. 5.10 even in these conditions, rotor angle estimation and sensorless control is achieved.

Although estimation using the MPCLPF is based on study state equations, the experimental result of the transient response in Fig. 5.11 shows sensorless control can be achieved when a step change is applied to the reference speed. In which case, rotor angle estimation and system transient response are acceptable.

The experimental results of the maximum power factor and maximum torque per ampere controls which are shown in Fig. 5.12 and Fig. 5.13 prove these control strategies can be achieved using the proposed method. As seen in these figures, the d axis current is set based on a control strategy and the d-q axes currents in the estimated and actual reference frame is in agreement.

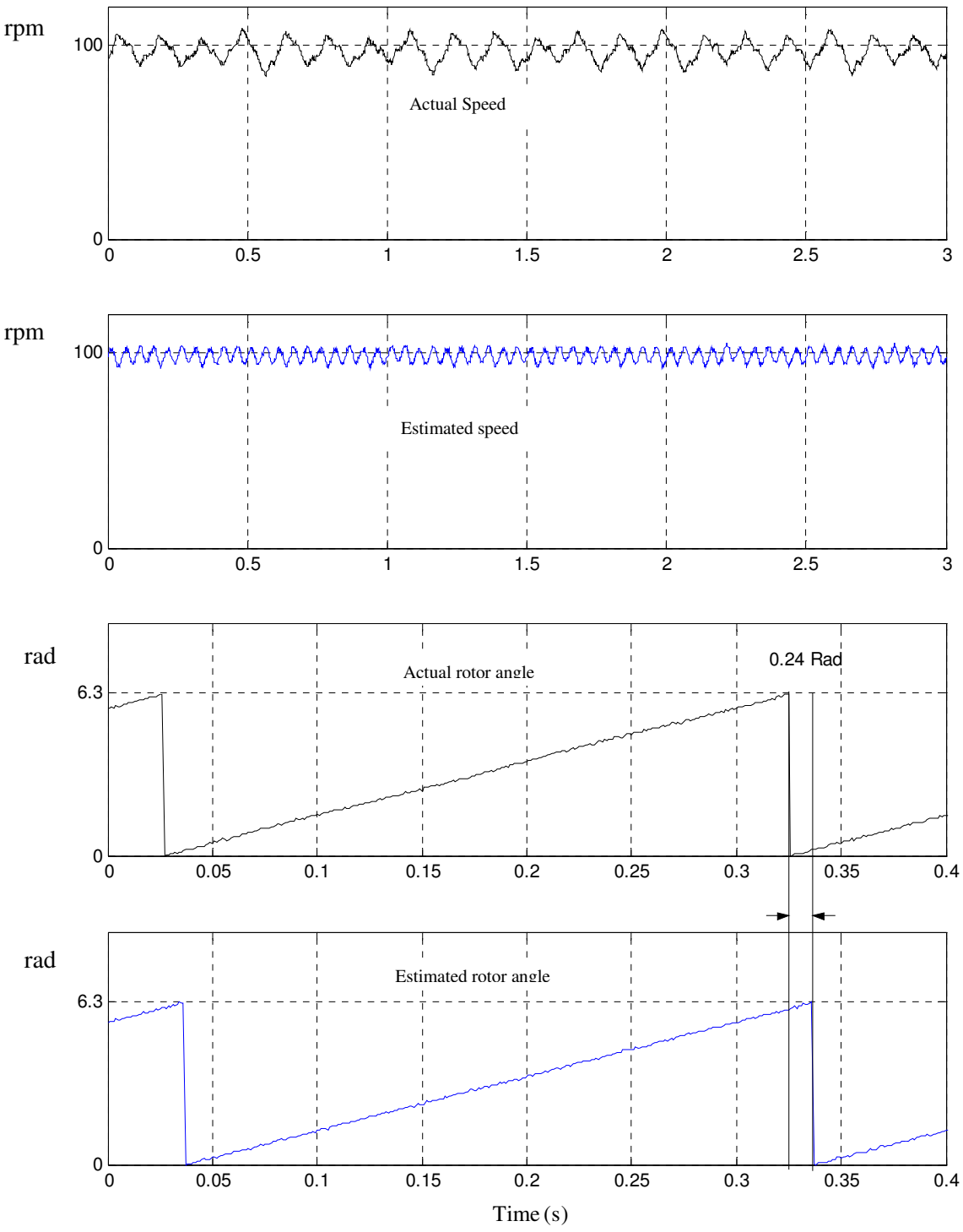

Fig. 5.7 Experimental results at 100 rpm using MPCLPF

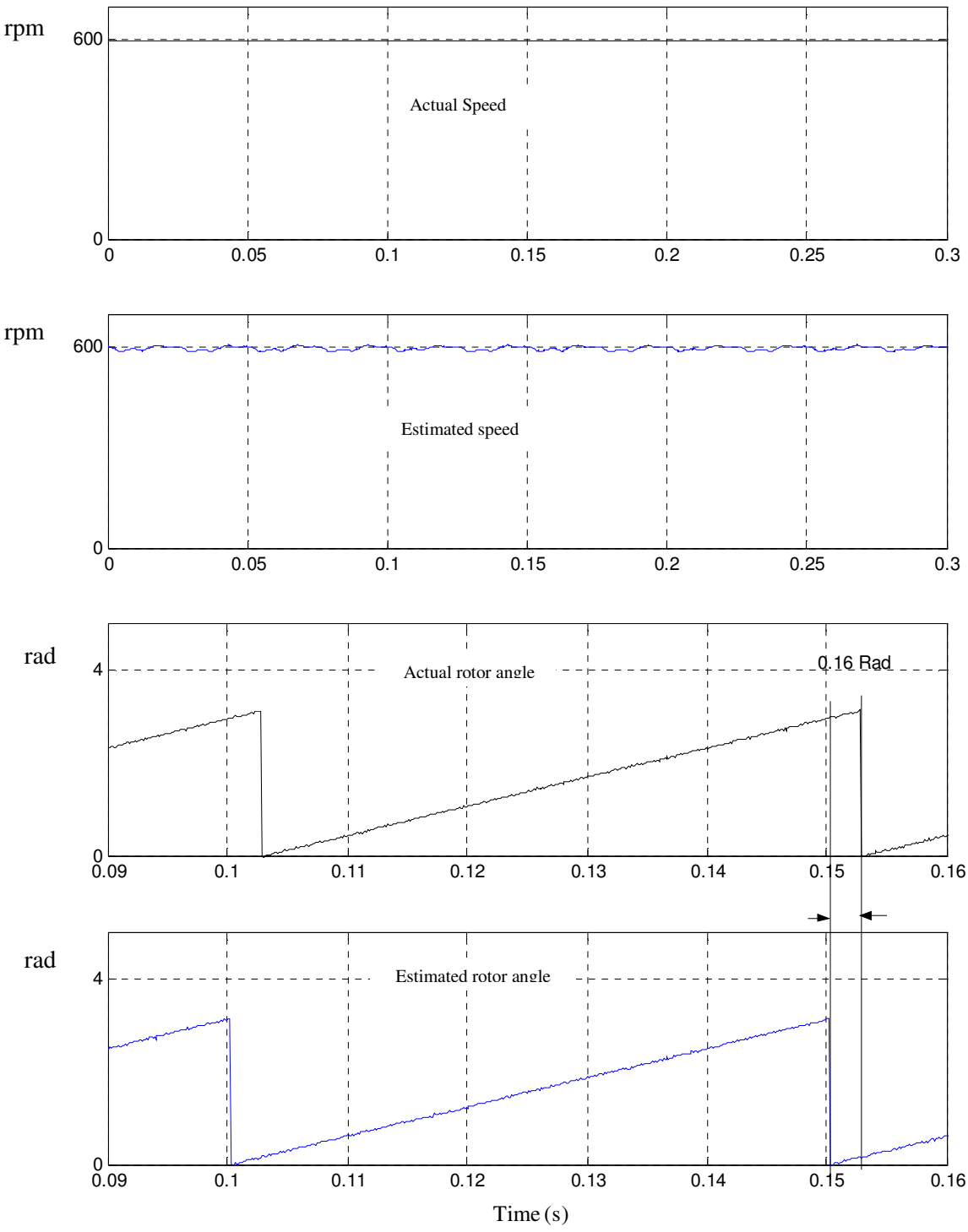

Fig. 5.8 Experimental results at 600 rpm using MPCLPF

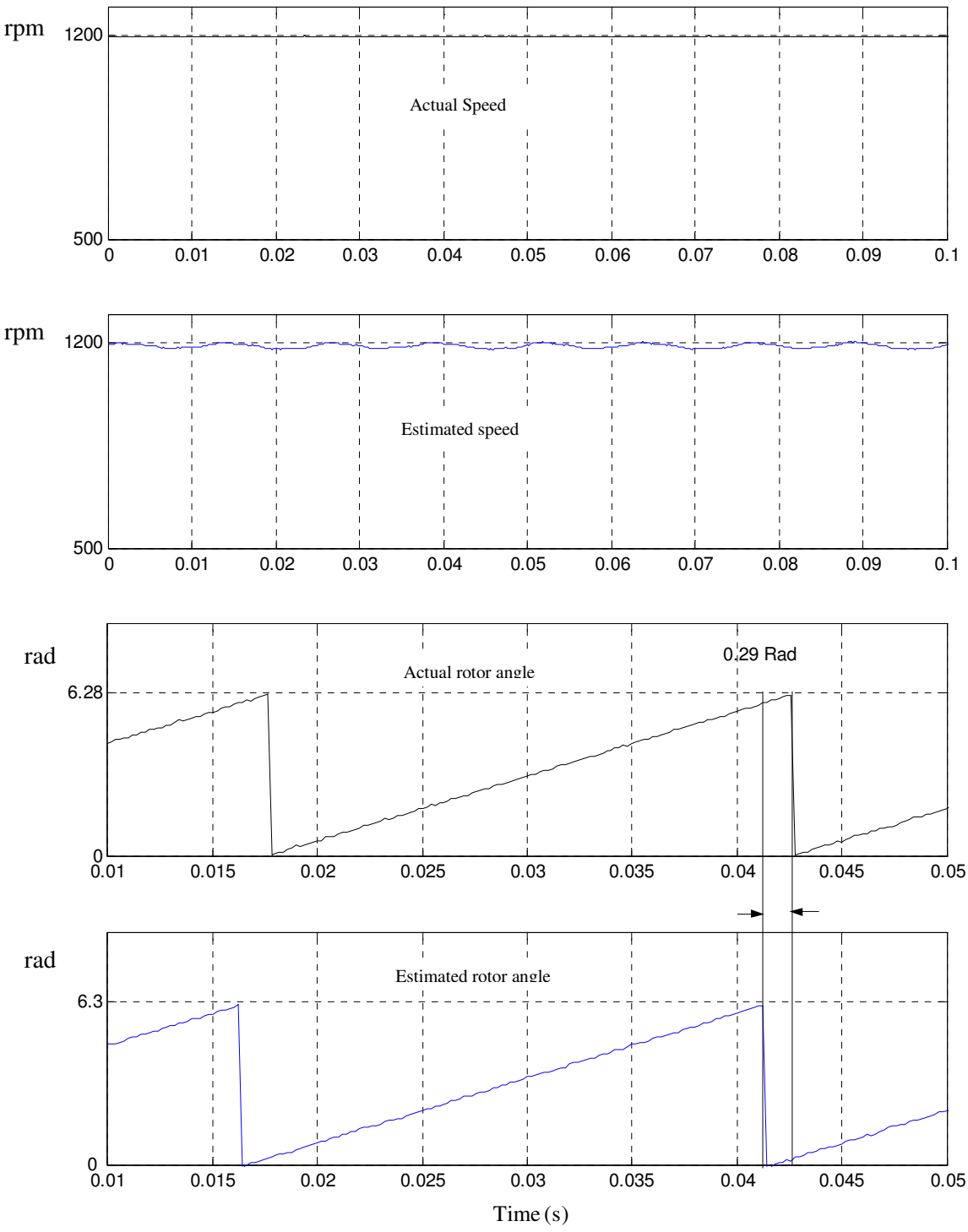

Fig. 5.9 Experimental results at 1200 rpm using MPCLPF

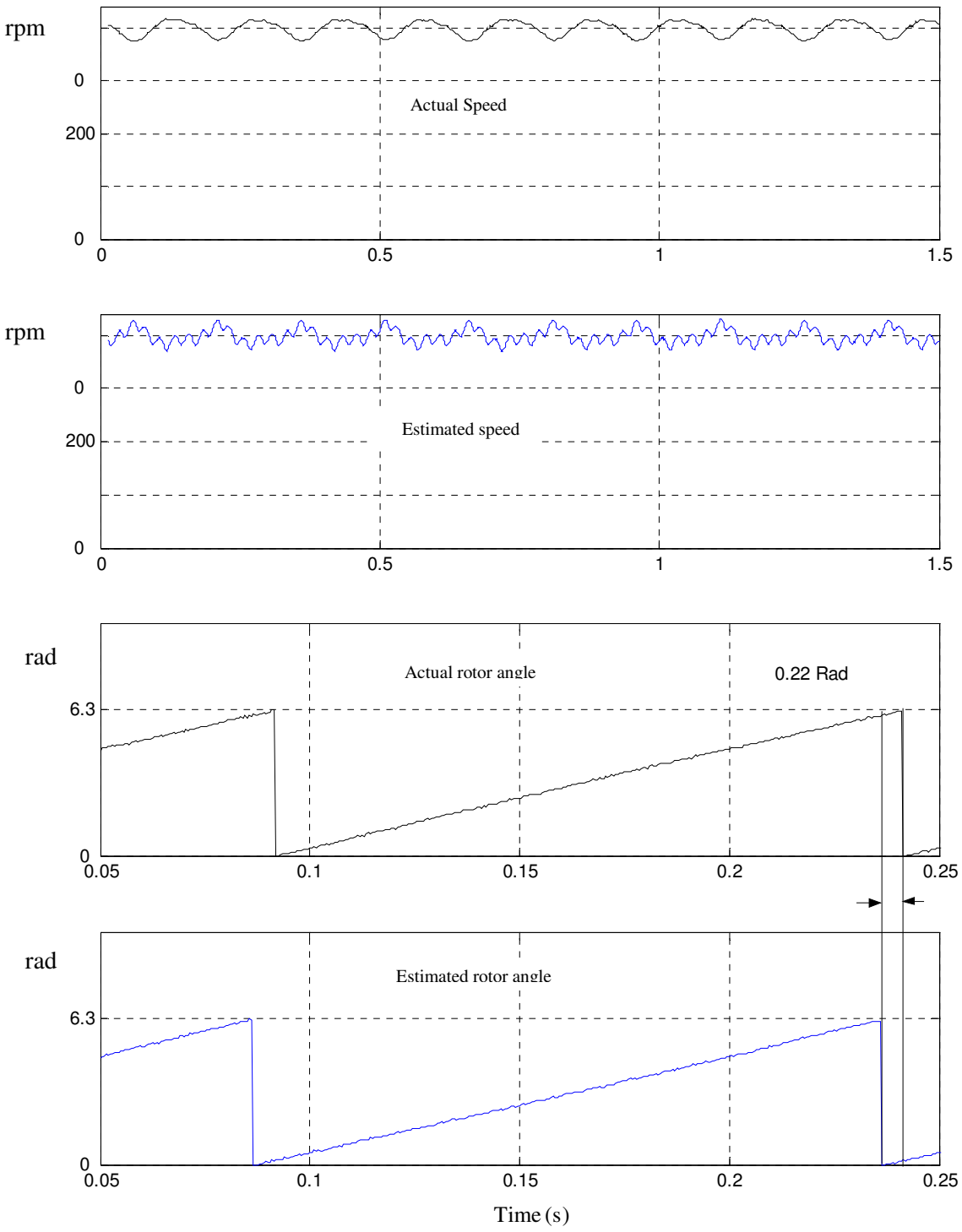

Fig. 5.10 Experimental results with 25 mA artificial dc offset

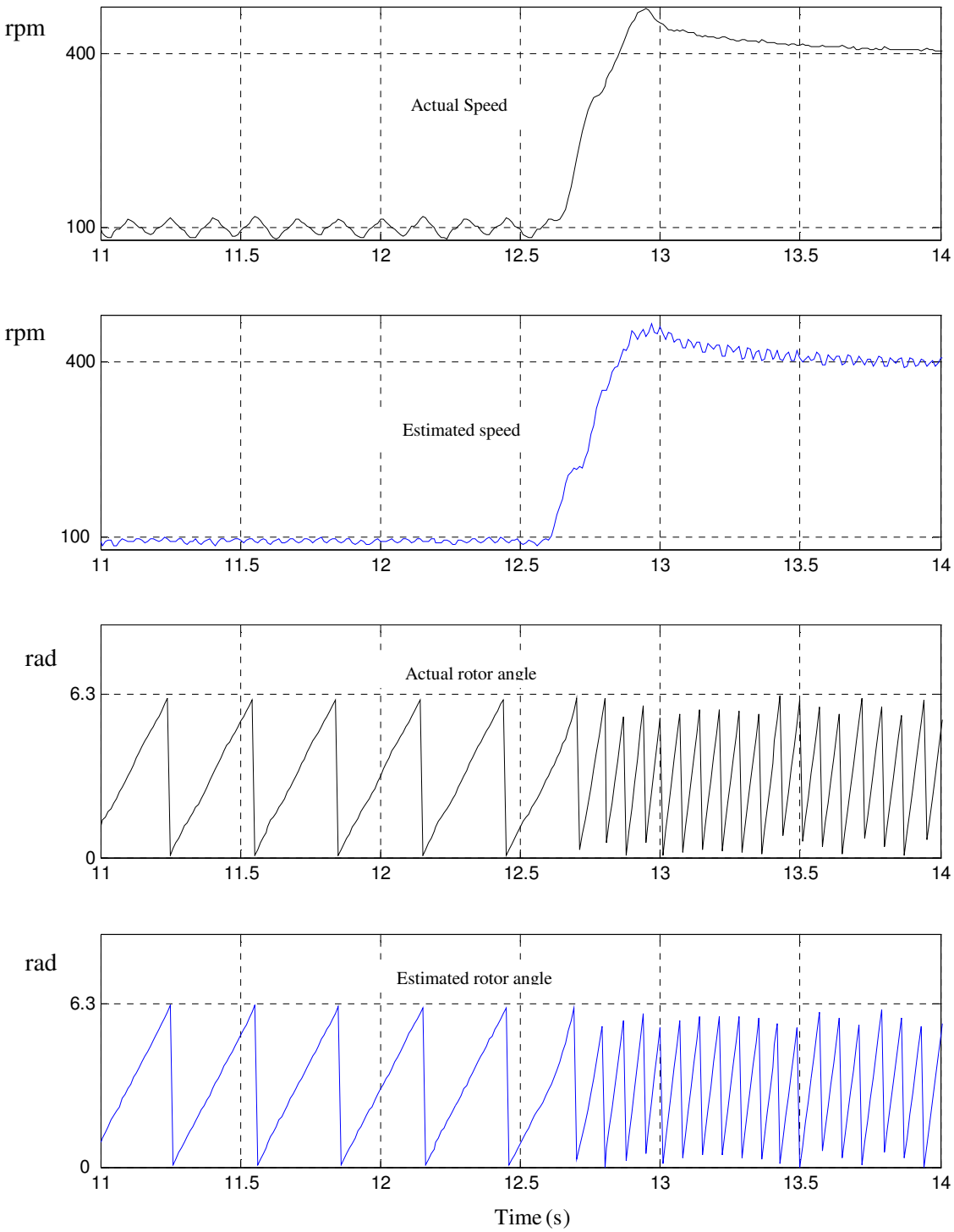

Fig. 5.11 Experimental results of transient response

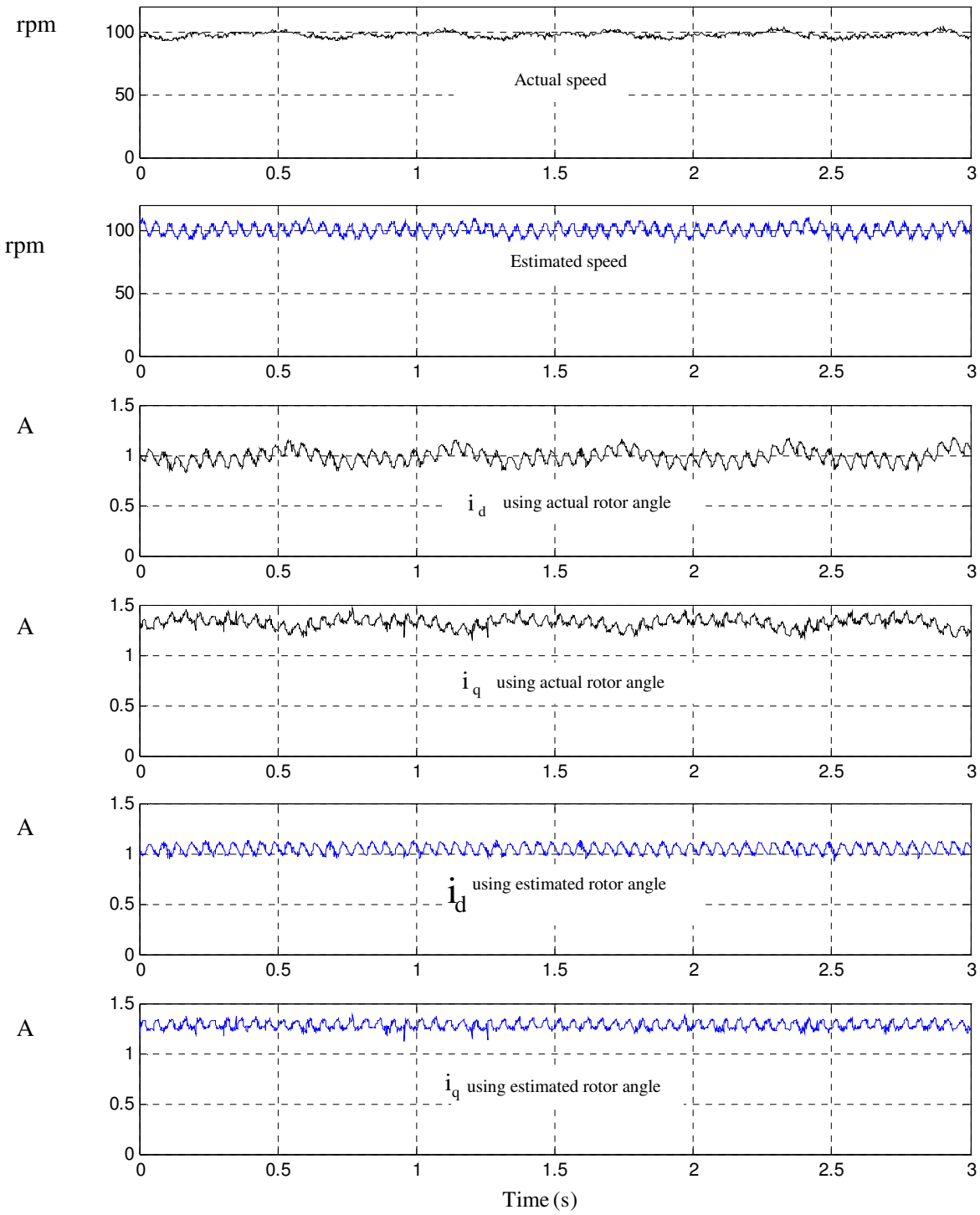

Fig. 5.12 Experimental results of maximum power factor control

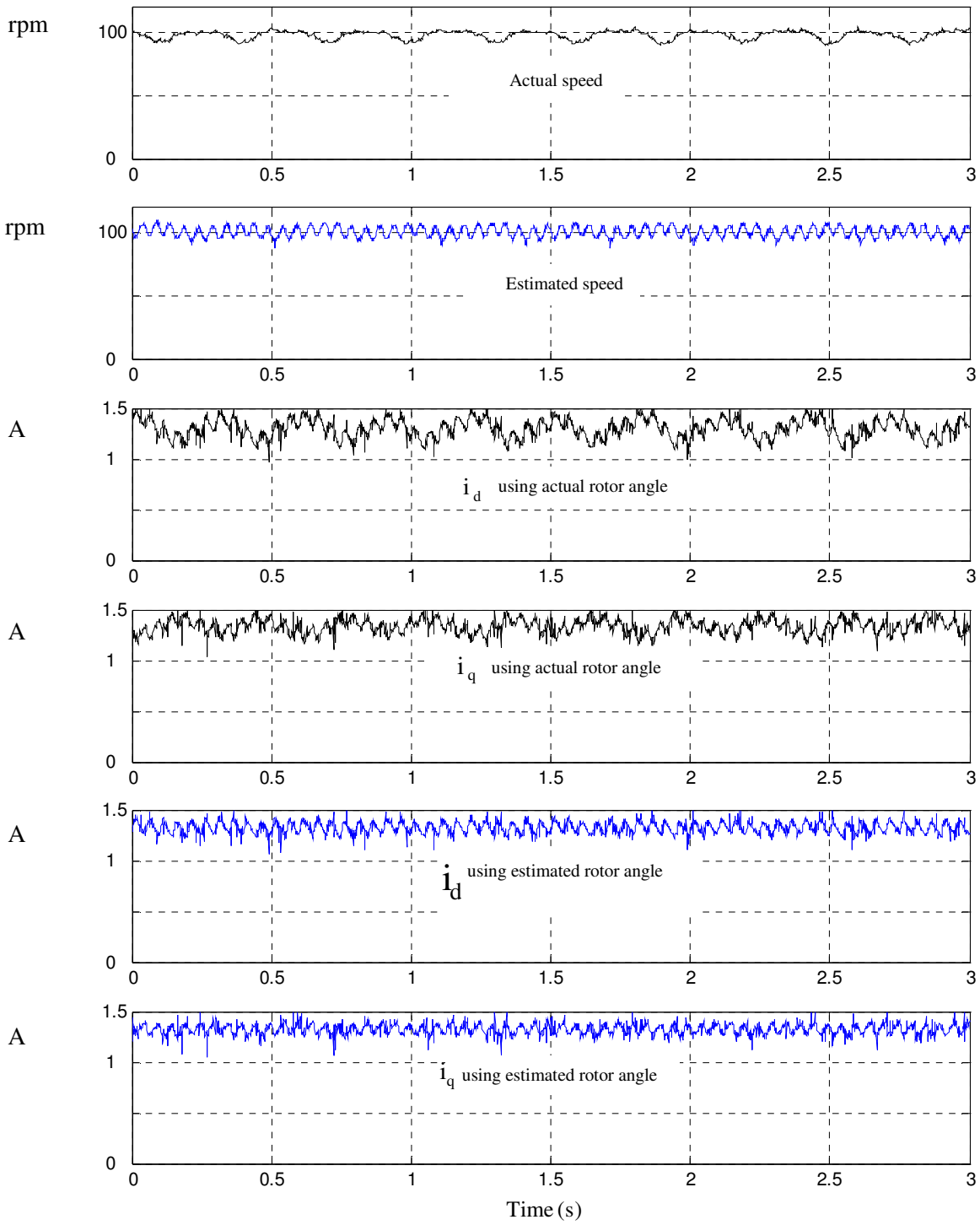

Fig. 5.13 Experimental results of maximum torque per ampere control

5.5.3 Experimental results using EPCLPF

As seen in previous subsection, the experimental results for speeds more than 2% of nominal speed are acceptable using MPCLPF. Because in these speeds the inverter voltage is much bigger than armature resistance voltage drop and rotor angle estimation is not difficult. But in low speed the estimation is difficult because the stator voltage is low, And noise, drift and nonlinearity is important. Thus to control motor in very low speeds and near zero speed hear, an EPCPLF is suggested.

The results for 100 rpm are shown in Fig. 5.14 using six stages EPCLPF. From the results, it is obvious that the estimation of speed is correct and the estimated and the actual rotor angle are agreed well, also the d-q axes currents in estimated and actual reference frame are agreed. On the other hand, it is seen that the error of angle estimation is compared with MPCLF, which have been shown in Fig 5.7.

Fig. 5.15 and Fig. 5.16 show the experimental result of the estimated and the actual rotor position in very low speed when the speed command is 5 rpm and 0.1 rpm, respectively. As seen in this figures the estimated rotor angle agree to the actual rotor angle at the near zero speed, and the estimator can calculate rotor angle at very low speed area. Thus sensorless control at very low speed area is possible.

The robustness of angle estimation against artificial disturbance, for injected drift, a 25 mA was added to the misused current signals while the motor was operating at 30% of rated torque, and as shown in Fig. 5.17 even in these conditions, estimated and actual rotor angle and estimated and actual d-q currents agree.

Like as MPCLPF, estimation using the EPCLPF is based on study state equations, however experimental result of the transient response shows sensorless control can be achieved when a step change is applied to the reference speed. Fig 5.18 shows the experimental results when a step change is applied to reference speed. As seen in this figure, the estimated d-q current and actual d-q current agree. Also these results show, angle estimation and system transient response are acceptable.

Fig. 5.19 and Fig. 5.20 show the experimental results when the motor direction is changed in high and low speed respectively. As seen in Fig. 5.19, for 200 rpm, change of motor direction is possible and estimated currents and actual currents agree and the amplitude of iq in both direction is same. Also the estimation of rotor angle and speed is acceptable. The results of direction change for 20 rpm is shown in Fig. 5.20. As seen in this figure, although the direction change is possible and estimated and actual values agree in both directions, there is a lag in change of motor direction. This delay is happen, because low pass filters should be reset before the motor direction could be changed. This lag increases in low speeds, because in this region the time constant of LPF is longer than high speed area and thus the response delay increases. It is a weak point of EPCLPF and some method should be suggested to solve this problem.

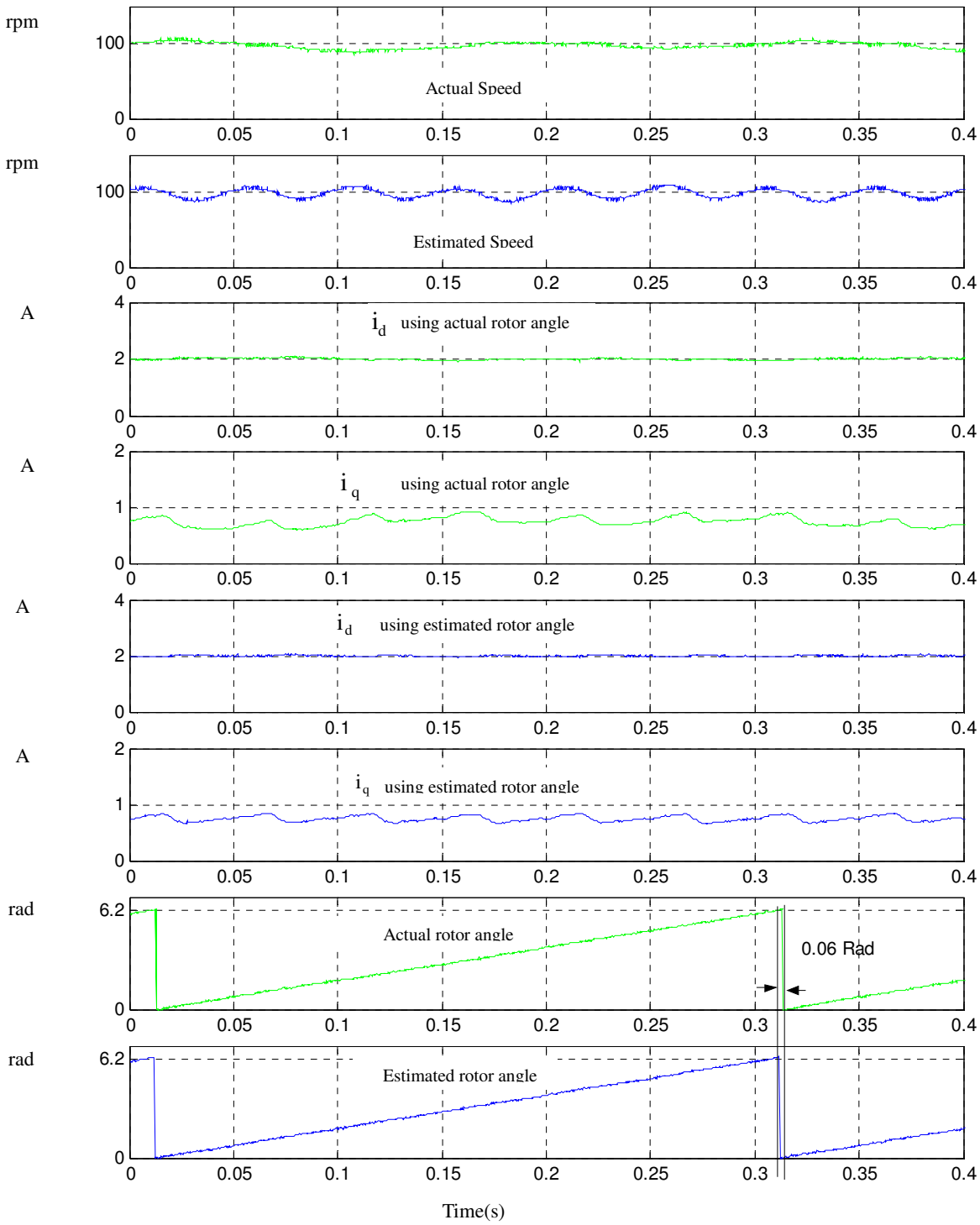

Fig. 5.14 Experimental results at 100 rpm using ECLPF

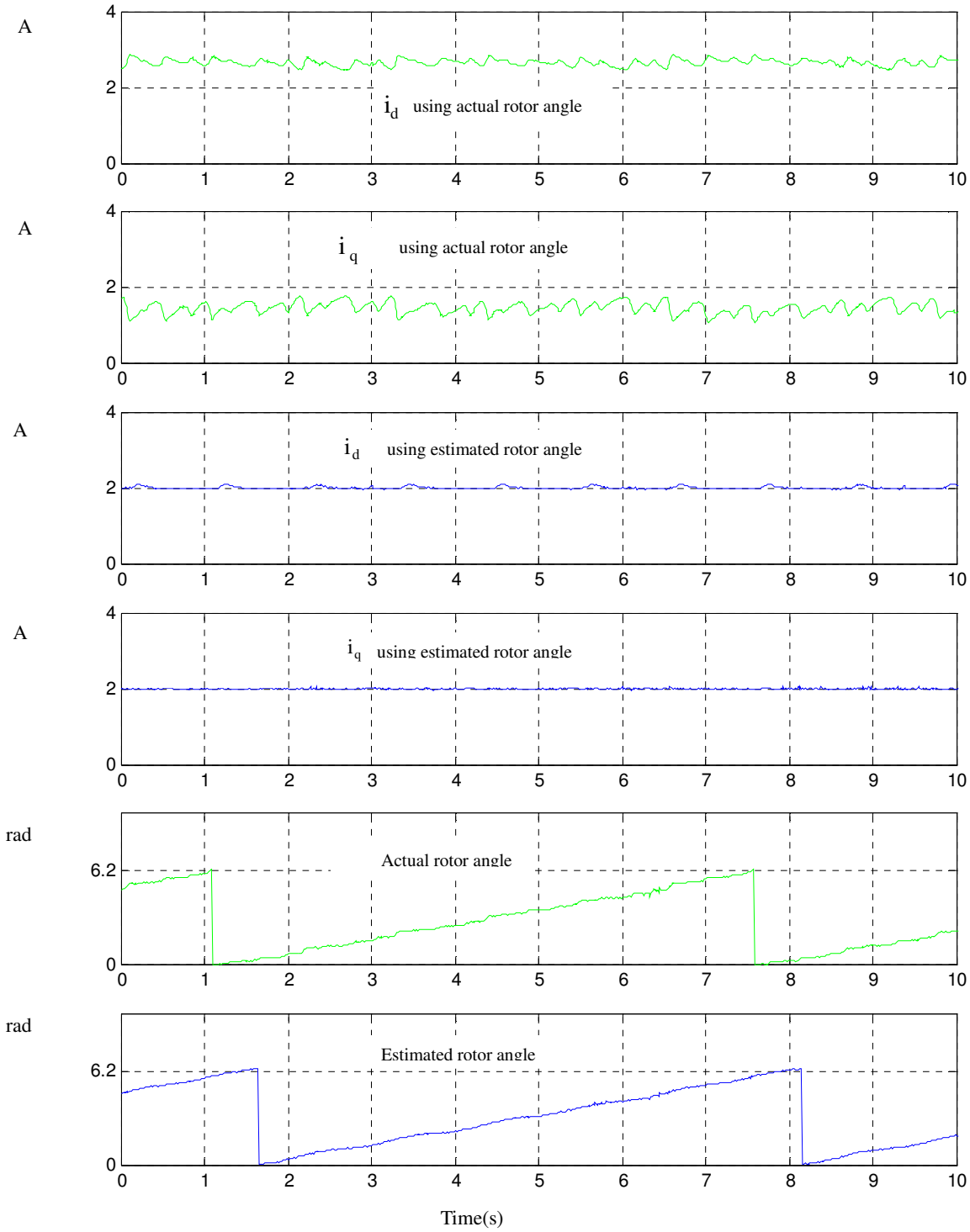

Fig. 5.15 Experimental results at 5 rpm using ECLPF

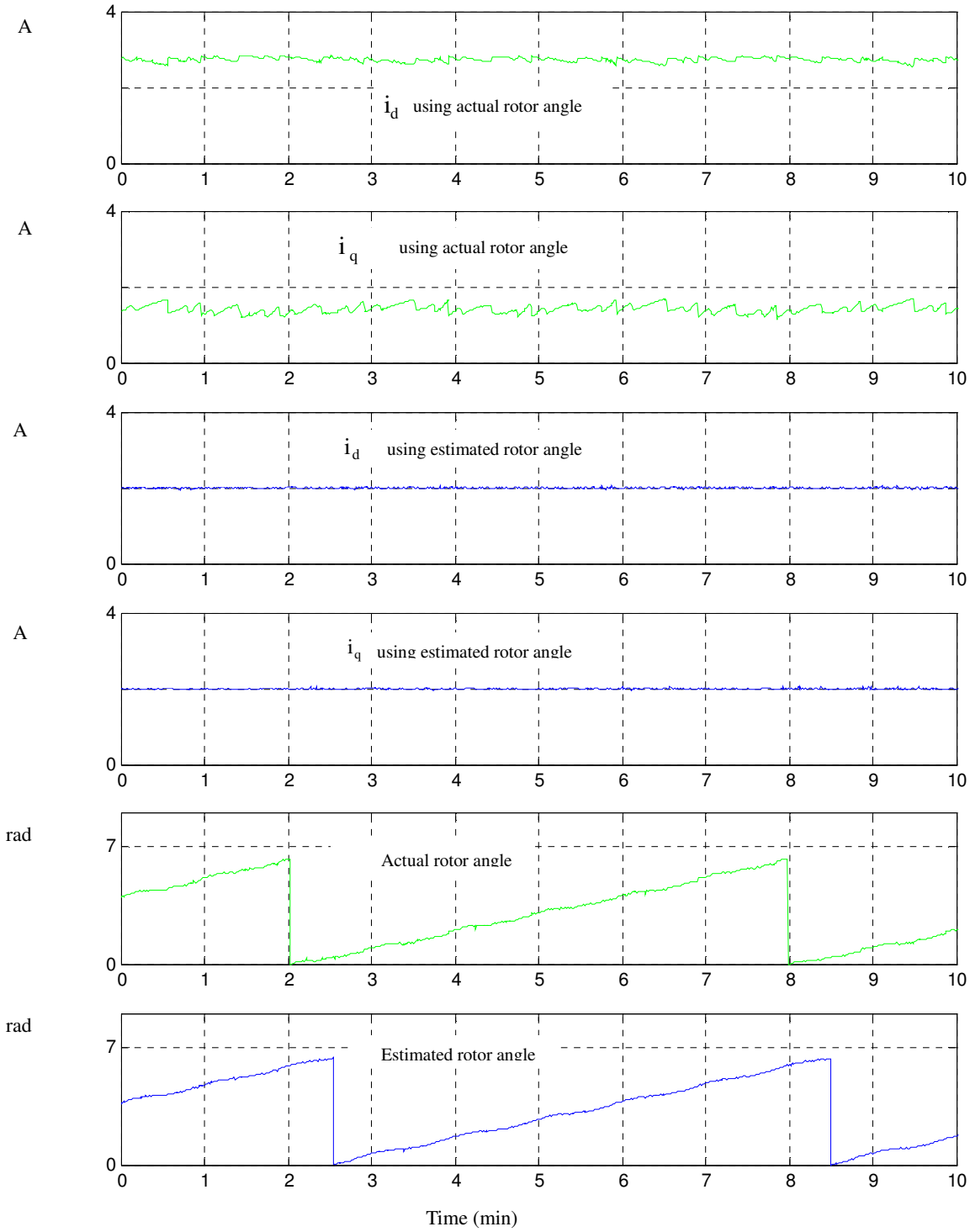

Fig. 5.16 Experimental results at 0.1 rpm using ECLPF

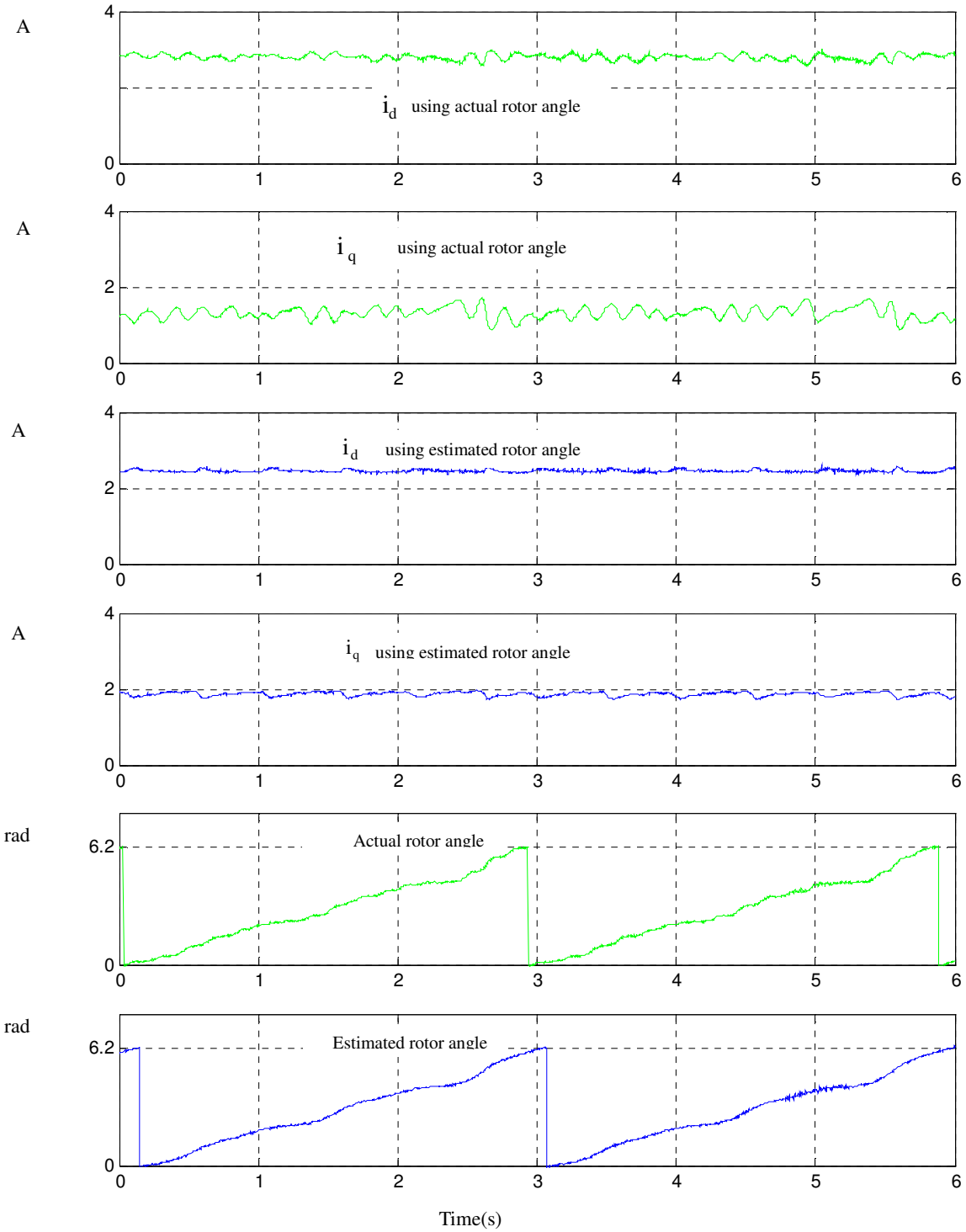

Fig. 5.17 Experimental results at 10 rpm with 25 mA artificial DC offset

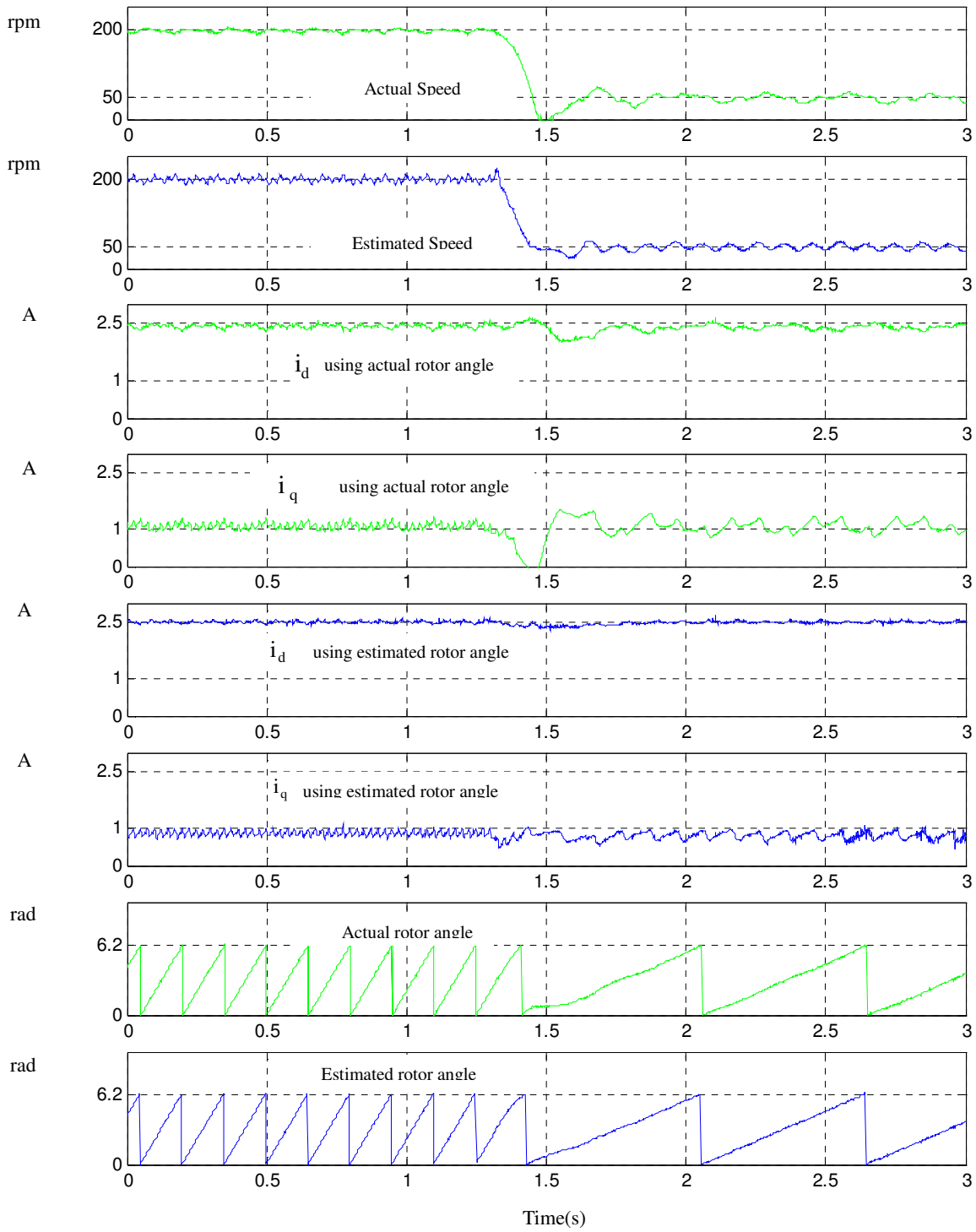

Fig. 5.18 Experimental results at 30% of rated load using ECLPF

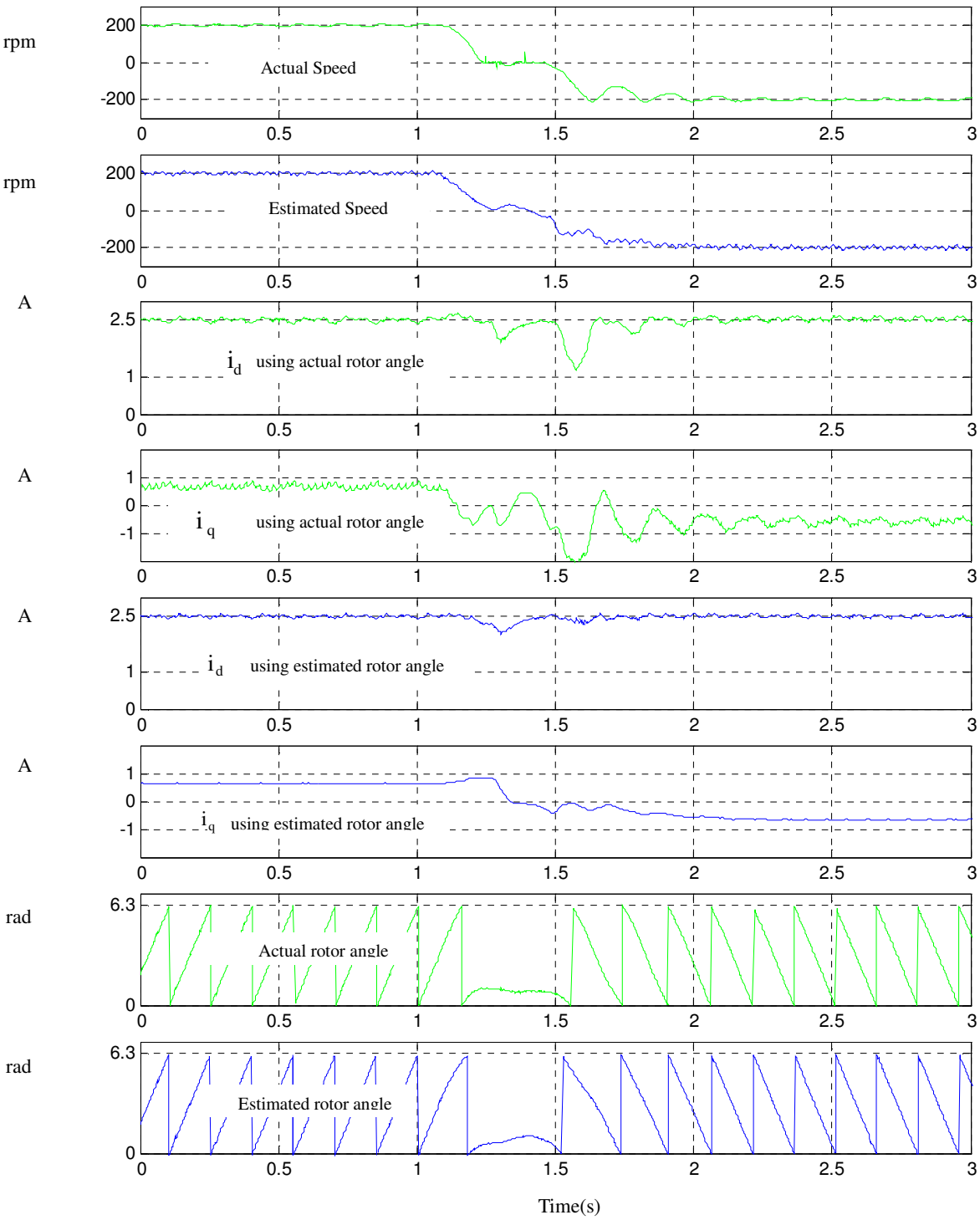

Fig. 5.19 Experimental result when the motor speed changes form 200rpm to -200rpm

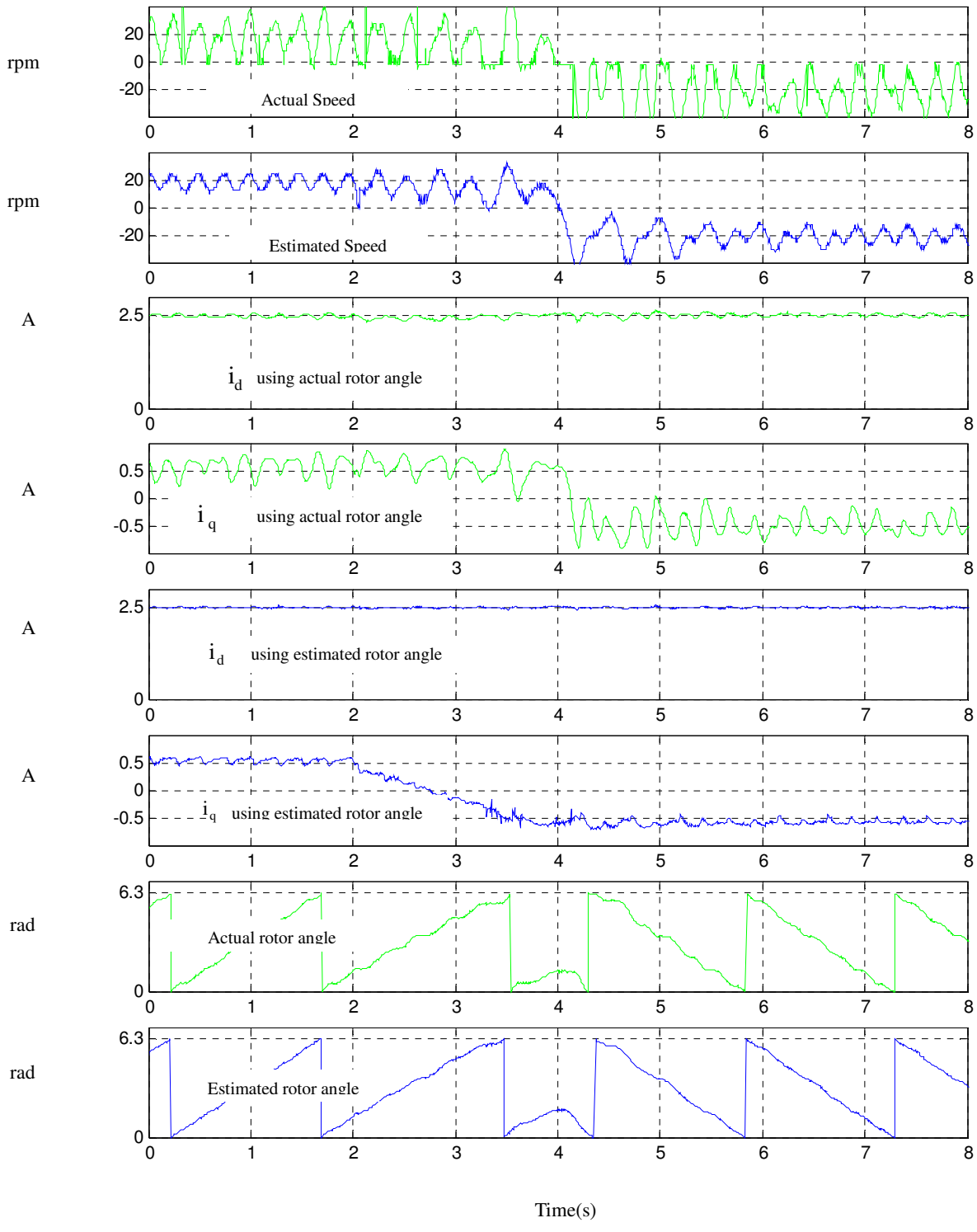

Fig. 5.20 Experimental result when the motor speed changes form 20rpm to -20rpm

To study the motor response at load changed condition, a step change in load torque is applied to motor. Fig. 5.21 and Fig. 5.22 show the experimental results, when a 30% of nominal load is added to motor. As seen in this figures the result of sensorless control conforms to sensor control and the regulation of motor speed without sensor is achieved as well as sensor control. Sensorless vector control is achieved and estimation is valid.

The experimental results when motor startup to 50 rpm in standstill condition is shown in Fig. 5.23. This figure shows the motor start up is achieved and the estimated and actual rotor angles converge after few revolutions.

The effect of LPFs stages on estimation accuracy was explained in chapter 3. As mentioned there, mathematical calculations show the effect of DC-offset is reduced when the stages of filters increase. To investigate the validity of these calculations, the practical experiments are done for 6, 9 and 12 stages of LPF. The experimental results which are shown in figures 5.21-5.23 the error of rotor angle calculation reduces when the stages of filters is increased. But increasing the filter stages cause an increasing in numerical calculation. For example for 12 stages EPCLPF the calculation is twice more than 6 stages EPCLPF. In this practical system, it is seen that 6 stages of LPF can solve the drift problem effectively.

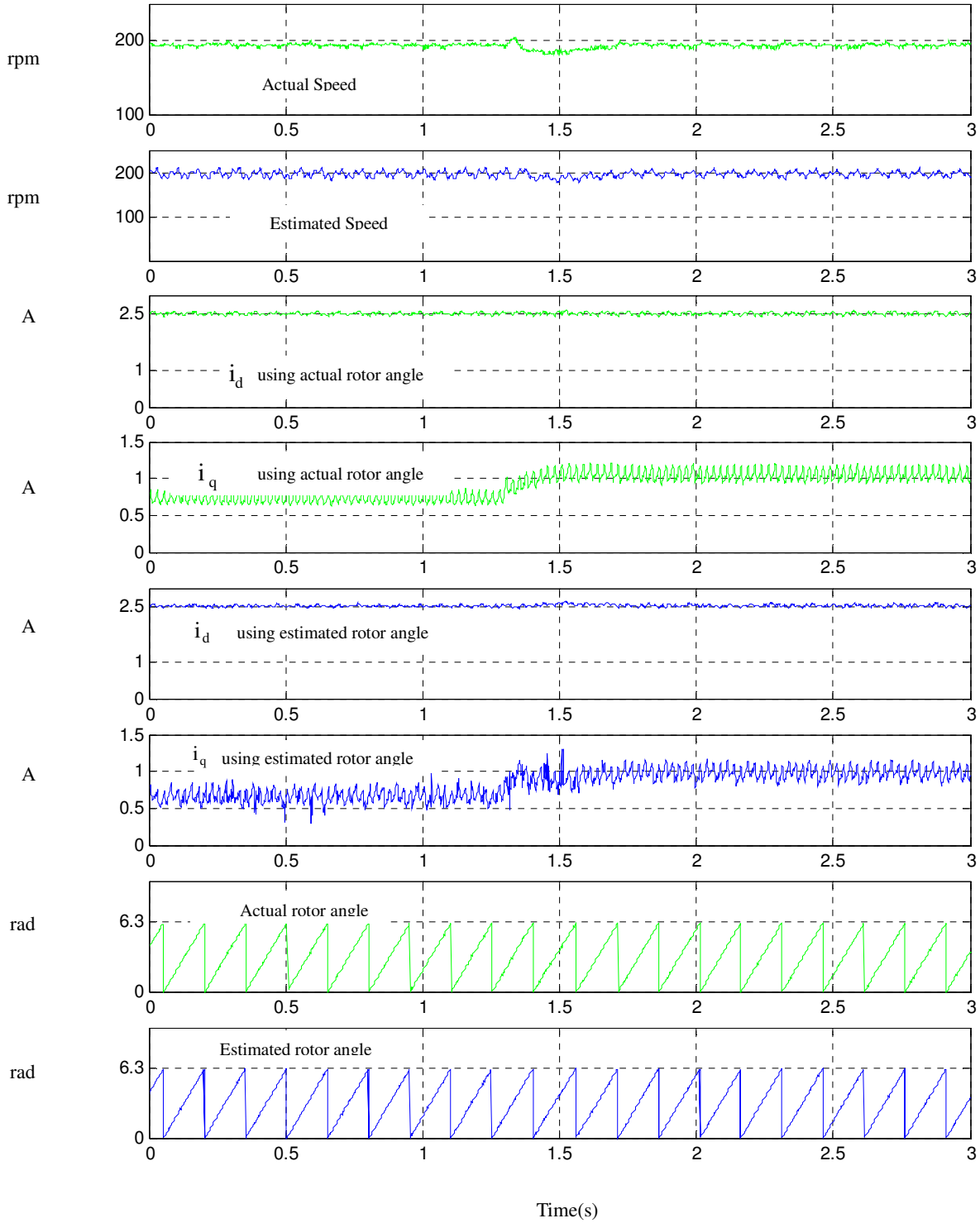

Fig. 5.21 Experimental result of sensor control when 30% of nominal load is added

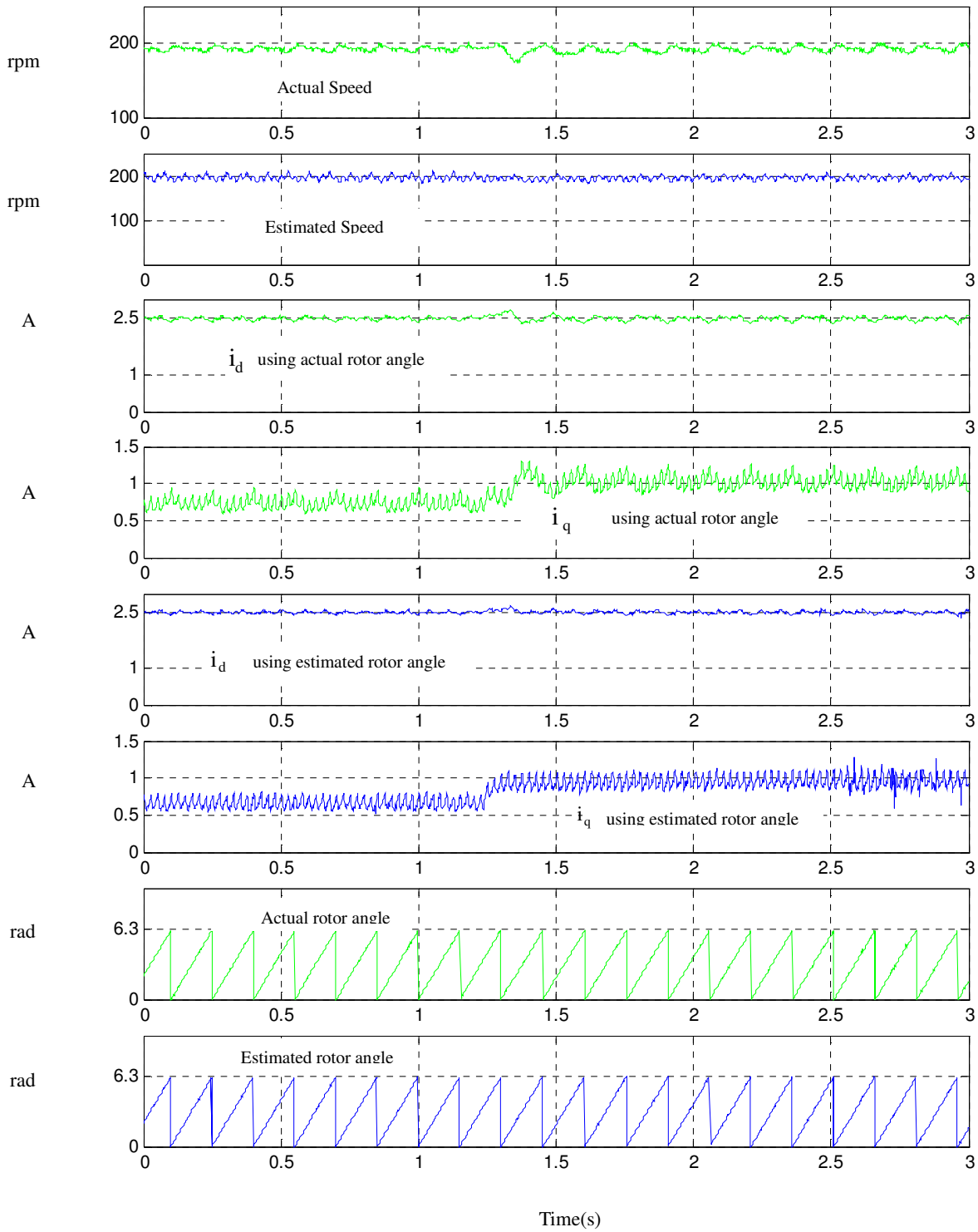

Fig. 5.22 Experimental result of sensorless control when 30% of nominal load is added

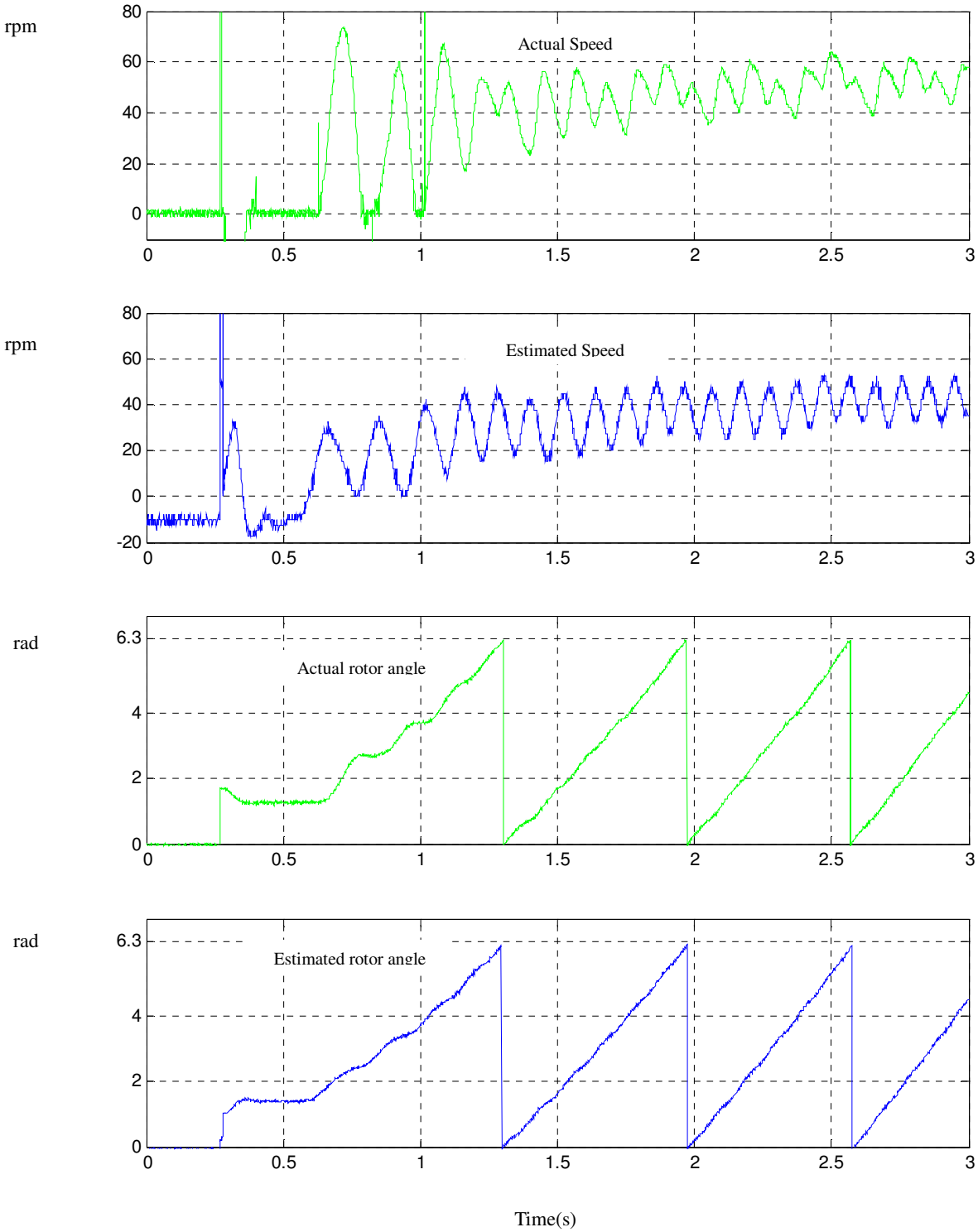

Fig. 5.23 Experimental results of startup at standstill condition

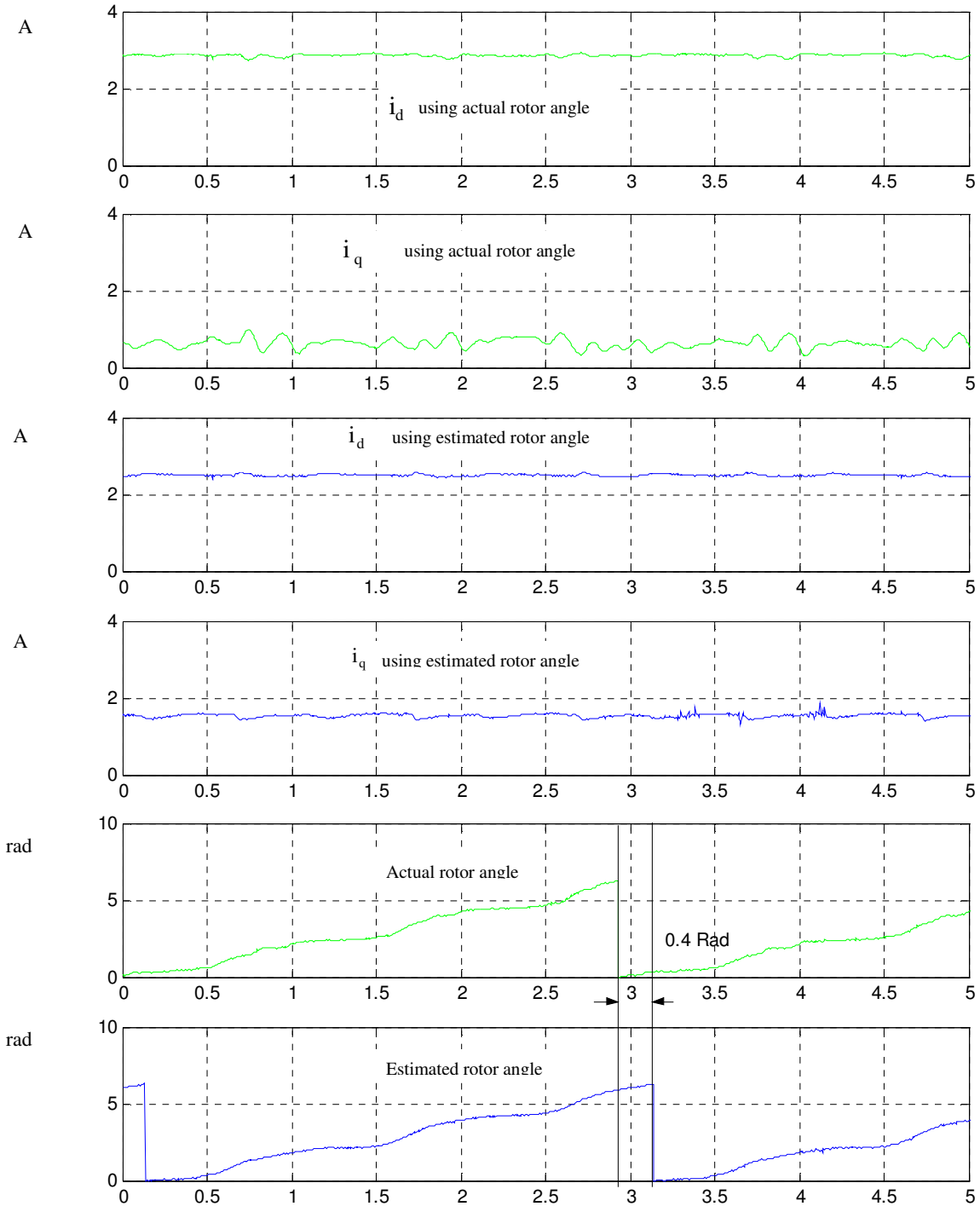

Fig. 5.24 .Experimental results at 10 rpm using 6 stages LPF

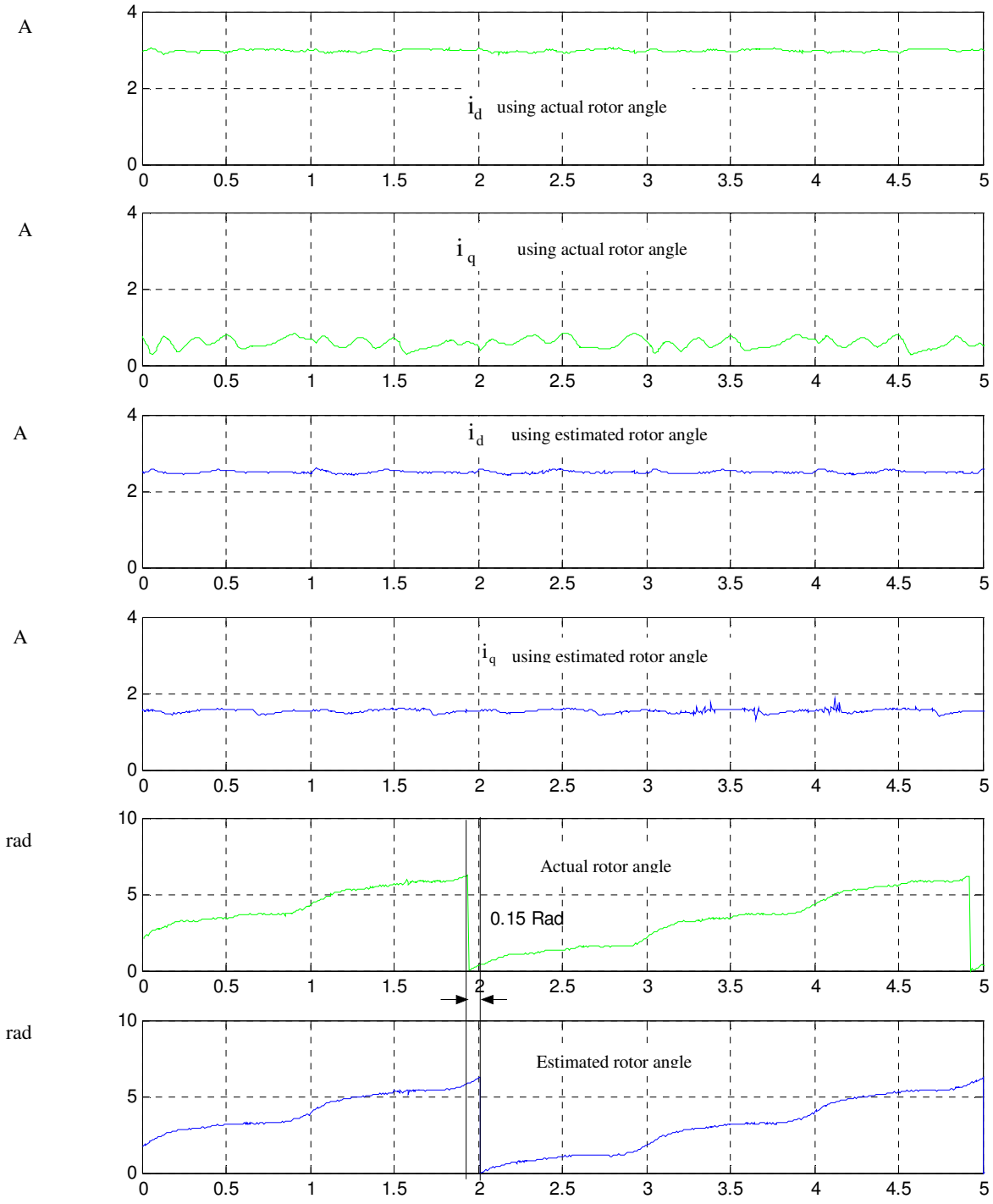

Fig. 5.25 Experimental results at 10 rpm using 9 stages LPF

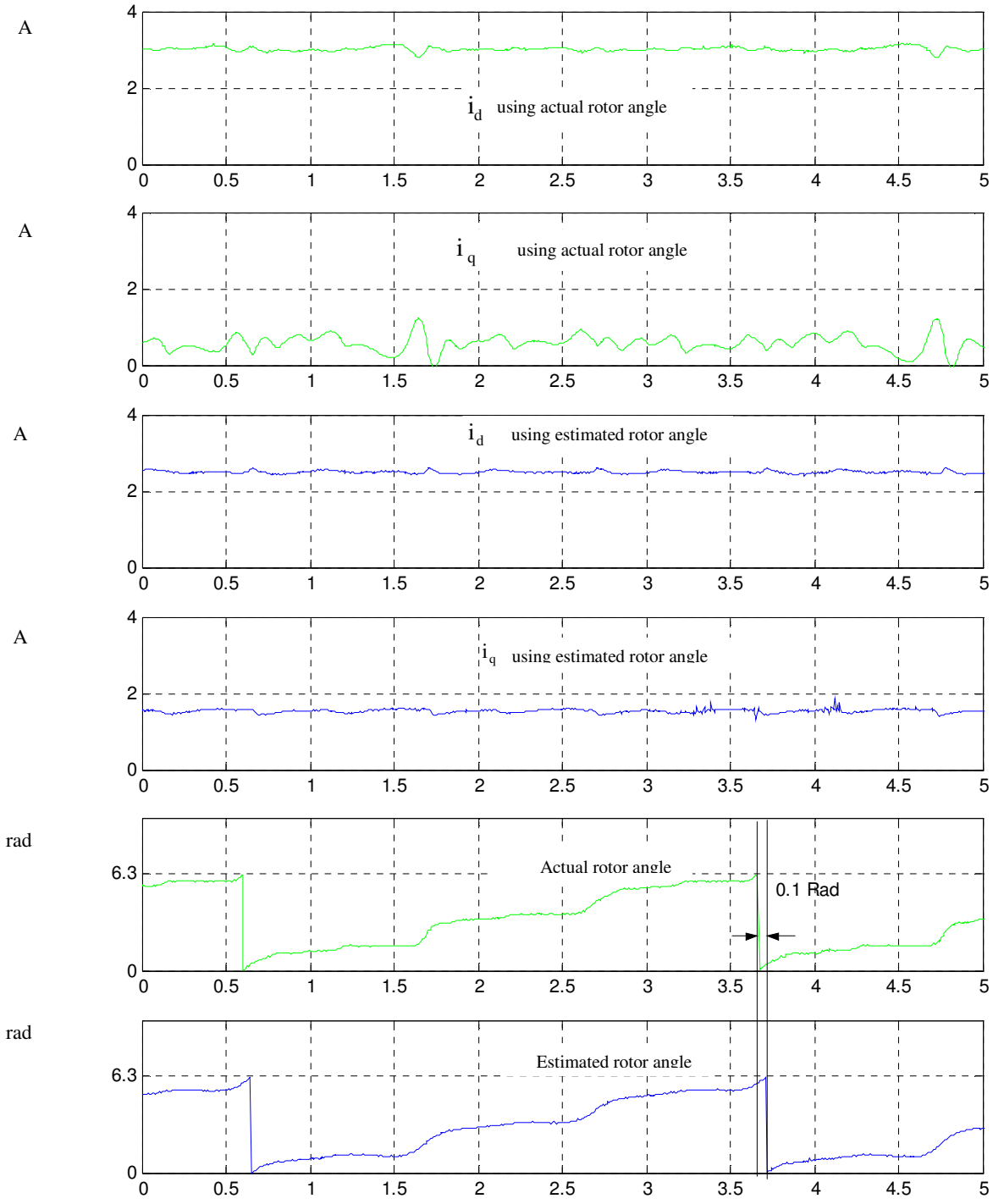

Fig. 5.26 Experimental results at 10 rpm using 12 stages LPF

Chapter 6

Conclusions

Although using fundamental models to estimate angles is the most straightforward approach and has several advantages, immunity to noise, offset and drift should be achieved using appropriate techniques else measurement noise and DC offset causes an increasing error in this estimator.

Use of programmable cascaded low pass filters (PCLPF) instead of pure integrators is another alternative method to reduce drift-error and it has previously been applied to the sensorless control of induction motors. In this thesis, this filter is adapted to estimate phase angle at low speed and near zero speed area in SYRM. To estimate rotor angle at low speed, modified programmable cascaded low pass filter (MPCLF) is presented. The problems of PCLPF are reduced because the PCLPF gain is eliminated in phase angle calculation.

In the next stage, the range of rotor angle calculation is expanded from near zero speed to high speed by proposing extended programmable cascaded low pass filters (EPCPLF). The performance of these filters is improved considerably by extending their stages and reduces its gain. Because the proposed method reduces the PCLPF drawbacks at low speed, effectively, the rotor angle estimation at very low speed is valid and thus, sensorless control at near zero speed is possible.

Although the rotor angle estimation using EPCPLF is possible at near zero speed, but it needs more calculation in compared with MPCLPF. Thus we suggest using EPCLPF in very low speed precise application while MPCPLF can be used in low speed application when we have limitation in hardware capacity.

Also the stator parameters are another mater in sensorless control and they must be defined precisely, else the sensorless vector control is not valid. While the stator resistance is important at phase angle calculation, especially in low speeds area, the motor inductances are required in load angle estimation and decoupling signal calculations. Thus a proper method for identifying motor parameter is essential. The nonlinearity of inverter also should be considered in reference voltage calculation.

To solve mentioned drawbacks in this thesis, an online parameter identification method which does not depend on estimation accuracy is suggested. In the proposed method, motor parameter

identification is done using a block pulse function (BPF), which saves calculation time compared with the other numerical analysis method, is used.

It is shown although the identified parameter is not dependent on angle difference of actual d-q axes and the estimated $\delta - \gamma$ axes. Hence, in this method, parameter identification is not affected by position estimation accuracy.

In this thesis a wide range speed sensorless vector control is achieved, using a combination of MPCLPF or EPCLPF and BPF-based parameter identification. Since the motor control strategy can be determined by regulating stator current in the d axis, several close loop self control methods, like as constant d-axis current control, maximum torque/ampere control and maximum power factor control are achieved using the identified parameters. Also the startup is possible without the torque jerk.

To achieve the proposed method, the experimental setup employs a PC-based system with real time Linux (RTLinux) as an operating system.

RTLinux can satisfy the system hardware and software constraints and also real time control can be achieved using this operating system. To acquire the data from the sensors and to send the gate signals to the system, an interface was designed by the Complex Programmable Logic Device (CPLD).

The experimental results show the proposed method performs well and speed and angle estimation is correct in a wide range of speeds.

The experimental result shows the parameter identification is valid in a wide range of speed, because this method is not affected by rotor angler estimation accuracy**.**

The experimental results using MPCLPF show that sensorless vector control is achieved at low speed regions, as well as, at high speeds using the proposed method. This results show the effect of the inverter nonlinearity increases at low speeds and this effect is considered as an additional nonlinear resistance series with armature circuit. Also these results show the estimated rotor angle agrees with the actual rotor angle and the accuracy of the angle estimation, which is shown is acceptable at high and low speeds. Several control strategies, like as maximum power factor and maximum torque per ampere can be achieved using the proposed method.

From the EPCLPF experimental results, it is obvious that the estimation of speed is correct and the estimated and the actual rotor angle are agreed well, also the d-q axes currents in estimated and actual reference frame are agreed. Also it is seen that, the estimated rotor angle agree to the actual rotor angle at the near zero speed, and the estimator can calculate rotor angle at very low speed area. Thus sensorless control at very low speed area is possible. The step responses of load torque and reference speed are acceptable, and change of motor direction without sensor is possible. Furthermore motor start up is achieved and the estimated and actual rotor angles converge rapidly. These results show although the effect of DC-offset is reduced when the stages of filters increase, 6 stages of LPF can solve the drift problem effectively.

For future researches following proposal is suggested.

1- Torque ripple is a major drawback in SYRM and to reduce its effect some technique should be used.

2- Although even in very low speed, sensorless control is possible using EPCLPF, there is a little difference between estimated and actual speed near zero speed. Therefore, more precise speed calculation method should be used in very low speed area.

3- As mentioned previously when the reference speed direction is changed, motor direction will not be changed immediately and there is a lag in change of motor speed direction. This delay is happen, because low pass filters should be reset before the motor direction could be changed. To solve this problem some method should be suggested.

4-The proposed method may be applied to sensorless vector control of PMSM or direct torque control of SYRM.

References

[1] G.K. Dubai, Fundamentals of electrical drive, Alpha Science International Ltd, 2001.

[2] I. Boldia, Vector control of AC drives, CRC Press Inc, 1992.

[3] W. Leonhard, Control of Electrical Drives, Springer, 2001.

[4] N. Mohan, Advanced Electric Drives: Analysis, Control and Modeling using Simulink, Mnpere, 2001.

[5] J. Holtz, "Developments in sensorless AC drive technology" proc of IEEE PEDS-Kuala Lumpur 2005, 2005, pp 9-16.

[6] P. Vas, Sensorless vector and direct torque control, Oxford University Press, 1998.

[7] B. K. Bose, Modern power electronics and drives, Prentice Hall PTR, 2002.

[8] T. Tamamura, Y. Honda, S. Morimoto, Y .Takeda, "Synchronous Reluctance motor when used Air-Condition Compressor Motor, a comparative study," Proc. of the IPEC-Tokyo 2000, pp. 654-659.

[9] B.H. Bae, S. K. Sul, "A Novel Dynamic Over modulation Strategy for Fast Torque Control of High-Saliency-Ratio AC Motor", IEEE Transactions on Industry Applications, Vol. 41, No. 4, pp 1013-1019 JULY/AUGUST 2005.

[10] C-G. Chen, T-H. Liu, M-T. Lin, C-A. Tai, "Position control of a sensorless synchronous reluctance motor" IEEE Transactions on Industrial Electronics, 2004, vol. 51, No. 1, pp. 15-25.

[11] S. Saha, T. Iijima, K. Narazaki, Y. Honda, "High speed sensorless control of synchronous reluctance motor by modulating the flux linkage angle," Proc of IPEC-Tokyo 2000, 2000, pp.643-648.

[12] Oh, Jae Yoon; Jung, Dal Ho, Flux barrier synchronous reluctance motor, United States Patent 6239526, 2001.

[13] S.Bolognani: "Torque angle calculator for sensorless reluctance motor drives", EPE Firenze, Vol.4 pp.13-17, 1991.

[14] R.Lagerquist, I.Boldea & T.J.Miller "Sensorless control of the synchronous reluctance motor" IEEE Trans on IAS Vol.30, pp.673-682, May/June 1994.

[15] A. Consoli, C. Cavallaro, G. Scarcella, A. Testa, "Sensorless torque control of SyncRel motor drives", IEEE Transactions on Power Electronics, Vol. 15, No. 1, pp.28 – 35 Jan. 2000.

[16] A. Consoli, F. Russo, G. Scarcella, A., Testa, "Low- and zero-speed sensorless control of

synchronous reluctance motors"IEEE Transactions on Industry Applications, Vol.35, No. 5, pp 1050 – 1057, Sept.-Oct. 1999.

[17] L. Kreindler, J. C. Moreira, A. Testa, T. A. Lipo, "Direct Field Orientation Controller Using the Stator Phase Voltage Third Harmonic", IEEE Transactions on Industry Applications, Vol. 30, NO. 2, Mar.-Apr. 1994.

[18] M.S. Arefeen, M. Eshani & T.A Lipo "Elimination of discrete position sensor for synchronous reluctance motor" Conf. Record of IEEE Power Electronics Specialists Conference, pp. 440-445, 1993.

[19] M.S. Arefeen, M. Eshani & T.A Lipo "An analisys of the accuracy of indirect shaft sensor for synchronous reluctance motor" IEEE Transactions on IAS Vol. 30. pp. 1202-1209, Sept. Oct. 1995.

[20] M.S. Arefeen, M. Eshani & T.A Lipo "Sensorless position measurement in synchronous reluctance motor" IEEE Transactions on IAS Vol. 30. pp. 1202-1209, Sept. Oct. 1995.

[21] M.S.Arefeen, M.Eshani & T.A Lipo "Indirect startup rotor position sensor for synchronous reluctance motor" Conf. Record of IEEE Power Electronics Specialists Conference, pp. 78-82, 1994.

[22] T.Mastsuo, T.A. Lipo "Rotor position detection scheme for synchronous RM based on current measurements" IEEE Trans. on IAS, Vol. 31, N.4, pp.860-868, July-August 1995.

[23] M.Schroedl, P.Weinmeiner "Sensorless control of reluctance machines at arbitrary operating condition including standstill" IEEE Trans. on Power Electronics, Vol.9, pp.225-231, March 1995.

[24] M. G. Jovanovi, R. E. Betz, D. Platt, "Sensorless Vector Controller for a Synchronous Reluctance Motor" IEEE Transactions on Industry Applications, Vol. 34, NO. 2, Mar.-Apr 1998.

[25] T. Hanamoto, A. Ghaderi, T. Fukuzawa, T. Tsuji, "Sensorless control of synchronous reluctance motor using modified flux linkage observer with an estimation error correct function," Proc. of the ICEM-2004,Sep 2004, Include CD-ROM.

[26] M.F. Rahman, M.E. Haque, L. Zhong, M. Nagrial, "A sensorless speed estimator for the direct torque control of an interior permanent magnet synchronous motor drive", Proc PEMD-2002, 4-7 June 2002, pp. 504 – 509.

[27] P. Vas, Artificial-Intelligence-Based Electrical Machines and Drives: Application of Fuzzy, Neural, Fuzzy-neural, and Genetic-Algorithm-based Techniques, Oxford University Press, 1999.

[28] Y. Dote, R. G. Hoft, Intelligent control power electronic system, Oxford University Press, 1998.

[29] P. L. Jansen, R. D. Lorenz, "Transducerless Position and Velocity Estimation in Induction and Salient AC Machines", IEEE Transactions on Industry Applications, Vol. 31, No. 2, Mar.-Apr 1995.

[30] J. I. Ha, S.J. Kang, S.K. Sul, "Position-Controlled Synchronous Reluctance Motor without

Rotational Transducer", IEEE Transactions on Industry Application, Vol. 35, No. 6, pp. 1393-1398, Nov.-Dec. 1999.

[31] E. Capecchi, P. Guglielmi, M. Pastorelli, A. Vagati, "Position-Sensorless Control of the Transverse-Laminated Synchronous Reluctance Motor", IEEE Transactions on Industry Application, Vol. 37, No. 6, Nov.-Dec. 2001.

[32] B.K. Bose, N.R. Patel, "A programmable cascaded low-pass filter based Flux synthesis for a stator flux-oriented vector-controlled Induction motor drive," IEEE Transaction on Industrial Electronics, Vol. 44., No. 1, pp.140-143, February 1997.

[33] A. Ghaderi, M. Ebrahimi, T. Hanamoto, "A novel compensation method of the flux estimation error in a stator flux oriented vector control of induction motors", Proc of ICEE-Sapporo, 2004, pp. 193-198.

[34] K. M. Rahman, S. Hiti, "Identification of Machine Parameters of a Synchronous Motor", IEEE Transaction on Industrial Electronics,Vol. 41, No. 2, Mar-Apr pp. 557-565, 2005.

[35] S. Ichikawa, A. Iwata, M. Tomita, S. Doki, S. Okuwa, "Sensorless control of synchronous reluctance motors using an on-line parameter identification method taking into account magnetic saturation" proc of the PESC 04,2004, pp. 3311-3316.

[36] A. Iwata, S. Ichikawa, M. Tomita, S. Doki, S. Okuwa, "Sensorless control of synchronous reluctance motors using an on-line parameter identification not affected by position estimation accuracy" IEEJ Transaction on Industry Application" Vol.124, No.12, pp.1205-1211, 2004. (Japanese)

[37] S. Ichikawa, M. Tomita, S. Doki, S. Okuma, "Sensorless Control of Synchronous Reluctance Motors Based on Extended EMF Models Considering Magnetic Saturation With Online Parameter Identification", IEEE Transaction on Industrial Electronics, Vol. 42, No. 5, Sep-Oct pp. 1264-1274, 2005.

[38] R. E. Betz, R. Lagerquist, M. Jovanovic, T. J. E. Miller, R. H. Middleton, "Control of Synchronous Reluctance Machines", IEEE Transaction on Industrial Electronics, Vol. 29, No. 6, Nov-Dec pp. 1110-1123, 1993.

[39] T. J. Summers, R. E. Betz, "Dead-Time Issues in Predictive Current Control" IEEE Transaction on Industrial Electronics, Vol. 40, No. 3, pp 835-844, May-June, 2004.

[40] B. Karanayil, M.F. Rahman, C. Grantham, "An implementation of a programmable cascaded low-pass filter for a rotor flux synthesizer for an induction motor drive", Proc of PESC-02. Vol. 4, 23-27 June, 2002 pp. 1965 – 1970.

[41] A. Ghaderi, T. Hanamoto, T. Tsuji," Sensorless Speed Control Method of Synchronous Reluctance Motor Using Programmable Cascade Low Pass Filter", Proc of JCEEE-2004, 2004, Include CD-ROM.

[42] A. Ghaderi, T. Hanamoto, T. Tsuji, "A Novel Implementation Method of a Programmable Cascaded Low Pass Filters for a Low Speed Sensorless Control of Synchronous Reluctance Motors", The Sixth IEEE International Conference on Power Electronics and Drive Systems (PEDS-2005), 28 Nov-1 Dec 2005, Kuala Lumpur-Malaysia, Include CD-ROM.

[43] A. Ghaderi, T. Hanamoto, T. Tsuji, "A Novel Implementation Of Low Speed Sensorless Vector Control Of Synchronous Reluctance Motors With A New Online Parameter Identification Approach", Proc of APEC-2006, 19-23 March 2006, Dallas-United State Include CD-ROM.

[44] A. Ghaderi, T. Hanamoto, T. Tsuji, Very Low Speed Sensorless Vector Control of Synchronous Reluctance Motors with a Novel Startup Scheme, 2007 IEEE Applied Power Electronics Conference and Exposition (APEC-2007), February 25 – March 1,Anaheim-United State.(Accepted)

[45] A. Ghaderi, T. Hanamoto, T. Tsuji, "A Novel Sensorless Low Speed Vector Control for Synchronous Reluctance Motors Using a Block Pulse Function-Based Parameter Identification", Journal of Power Electronics (JPE), Vol.6, No.3, pp.235-244, July 2006.

[46] Z. Jiang, W.r Schaufelberger, Block Pulse Functions and Their Applications in Control Systems, Springer-Verlag, 1992.

[47] T. Hanamoto, A. Ghaderi, T. Tsuji, "RTLinux Based Online Real Time Simulator of SPMSM using the Block Pulse Approximation" proc of IEEE PEDS-Kuala Lumpur 2005, 2005, pp 1118-1122.

[48] http://www.rtlinux.org

[49] P. Neti, S. Nandi "Determination of effective air-gap length of synchronous reluctance motors (SynchRel) from experimental data", IEEE Transactions on Industry Applications, Vol. 42, No.2, pp. 454 – 464, March-April 2006.

[50] T. Matsuo, A. El-Antably, T. A. Lipo, "A New Control Strategy for Optimum-Efficiency Operation of a Synchronous Reluctance Motor", IEEE Transactions on Industry Applications, Vol. 33, No. 5, Sep-Oct 1997.

[51] S. Morimoto, M. Sanada, Y. Takeda, " Performance of PM-Assisted Synchronous Reluctance Motor for High-Efficiency and Wide Constant-Power Operation", IEEE Transactions on Industry Applications, Vol. 37, No. 5, Sep-Oct 2001.

[52] P. Guglielmi, M. Pastorelli, .A. Vagati, "Cross-Saturation Effects in IPM Motors and Related Impact on Sensorless Control", IEEE Transactions on Industry Applications, Vol. 42, No. 6, Nov-Dec, 2006.

[53] A. Boglietti, A. Cavagnino, M. Pastorelli, D. Staton, A. Vagati, "Thermal Analysis of Induction and Synchronous Reluctance Motors" , IEEE Transactions on Industry Applications, Vol. 42, No. 3, pp. 675-680,May-June 2006.

[54] H. D. Lee, S. J. Kang, S. K. Sul, "Efficiency-Optimized Direct Torque Control of Synchronous Reluctance Motor Using Feedback Linearization", IEEE Transactions on Industrial, Vol. 46, No. 1, Feb, pp. 192-198, 1999.

[55] M. Sanada, K. Hiramoto, S. Morimoto, Y. Takeda, "Torque ripple improvement for synchronous reluctance motor using an asymmetric flux barrier arrangement", IEEE Transactions on Industry Applications, Vol. 40, No.4, pp. 1076-1082, July-Aug. 2004.

[56] P. C. Krause, O. Wasynczuk, S. D. Sudhoff, Analysis of Electric Machinery and Drive

Systems, Wiley-IEEE Press, 2002.
[57] T. Matsuo, T. A. Lipo, "Rotor Position Detection Scheme for Synchronous Reluctance Motor Based on Current Measurements", IEEE Transactions on Industry Applications, Vol. 31, No. 4, Jul-Aug 1995.
[58] A. J. Peyton, V. Walash, V., Analog Electronics with Op Amp a Source Book of Practical circuits, Cambridge University Press, 1996.
[59] J. Williams, Analog Circuit Design Art Science and Personalizes, Butterworth Heinemann Inc, 1994.
[60] C. L. Phillips, H. T. Nagle, Digital Control System Analysis and Design, Prentice Hall, 1984.
[61] I. D. Landun, System Identification and Control Design, Prentice Hall, 1990.
[62] T. Hanamoto, A. Ghaderi, T. Tsuji "RTLinux Based Speed Control System of SPMSM with an Online Real Time Simulator", IEEJ Transactions on Industry Applications, Vol.126, pp.453-458, April, 2006.
[63] http://rtic-lab.sourceforge.net/
[64] http://www.altera.com

List of publications

Major papers

1) A. Ghaderi, T. Hanamoto, T. Tsuji, “A Novel Sensorless Low Speed Vector Control for Synchronous Reluctance Motors Using a Block Pulse Function-Based Parameter Identification”, **Journal of Power Electronics (JPE),** Vol.6, No.3, pp.235-244, July 2006.

2) A. Ghaderi, T. Hanamoto, T. Tsuji, Very Low Speed Sensorless Vector Control of Synchronous Reluctance Motors with a Novel Startup Scheme, 2007 IEEE Applied Power Electronics Conference and Exposition (APEC-2007), February 25 – March 1,Anaheim-United State**.**

3) A. Ghaderi, T. Hanamoto, T. Tsuji, A Novel Implementation Of Low Speed Sensorless Vector Control Of Synchronous Reluctance Motors With A New Online Parameter Identification Approach, 2006 IEEE Applied Power Electronics Conference and Exposition (APEC-2006), 19-23 March 2006, Dallas-United State.

4) A. Ghaderi, T. Hanamoto, T. Tsuji, A Novel Implementation Method of a Programmable Cascaded Low Pass Filters for a Low Speed Sensorless Control of Synchronous Reluctance Motors, The Sixth IEEE International Conference on Power Electronics and Drive Systems (PEDS-2005), 28 Nov-1 Dec 2005, Kuala Lumpur-Malaysia.

5) A. Ghaderi, M. Ebrahimi, T. Hanamoto, A Novel Compensation Method of the Flux Estimation Error in a Stator Flux Oriented Vector Control of Induction Motors, 10th International Conference on Electrical Engineering (ICEE2004), July 4-8, 2004, Sapporo , Japan.

Other Related papers

1) T. Hanamoto, A. Ghaderi, & T. Tsuji "RTLinux Based Speed Control System of SPMSM with an Online Real Time Simulator", **IEEJ Transactions on Industry Applications,** Vol.126, pp.453-458, April, 2006.

2) A. Ghaderi, T. Hanamoto, T. Tsuji, Sensorless Speed Control Method of Synchronous Reluctance Motor Using Programmable Cascade Low Pass Filter ,Joint Conference of Electrical and Electronic Engineers in Kyushu by IEEE Fukuoka (JCEEE-2004), 2004, Kagoshima-Japan.

3) T. Hanamoto, A. Ghaderi, T. Fukuzawa, T. Tsuji, Sensorless control of synchronous reluctance motor using modified flux linkage observer with an estimation error correct function,16th International Conference on Electrical Machine (ICEM-2004), 2004, Poland.